

Manuscript Number: ER-14-721R2

Title: Silver Nanoparticles Affect on Gene Expression of Inflammatory and Neurodegenerative Responses in Mouse Brain Neural Cells

Article Type: Research Paper

Section/Category: Toxicology

Keywords: silver nanoparticle; inflammation; gene expression; neurodegenerative disorder; Alzheimer's disease.

Corresponding Author: Dr. Chun-Yu Chuang, PhD

Corresponding Author's Institution: National Tsing-Hua University

First Author: Chin-Lin Huang, Master

Order of Authors: Chin-Lin Huang, Master; I-Lun Hsiao, PhD; Ho-Chen Lin, PhD; Chu-Fang Wang, PhD; Yuh-Jeen Huang, PhD; Chun-Yu Chuang, PhD

Abstract: Silver nanoparticles (AgNPs) have antibacterial characteristics, and currently are applied in Ag-containing products. This study found neural cells can uptake 3-5 nm AgNPs, and investigated the potential effects of AgNPs on gene expression of inflammation and neurodegenerative disorder in murine brain ALT astrocytes, microglial BV-2 cells and neuron N2a cells. After AgNPs (5, 10, 12.5 $\mu\text{g}/\text{ml}$) exposure, these neural cells had obviously increased IL-1 β secretion, and induced gene expression of C-X-C motif chemokine 13 (CXCL13), macrophage receptor with collagenous structure (MARCO) and glutathione synthetase (GSS) for inflammatory response and oxidative stress neutralization. Additionally, this study found amyloid- β (A β) plaques for pathological feature of Alzheimer's disease (AD) deposited in neural cells after AgNPs treatment. After AgNPs exposure, the gene expression of amyloid precursor protein (APP) was induced, and otherwise, neprilysin (NEP) and low-density lipoprotein receptor (LDLR) were reduced in neural cells as well as protein level. These results suggested AgNPs could alter gene and protein expressions of A β deposition potentially to induce AD progress in neural cells. It's necessary to take notice of AgNPs distribution in the environment.

Date: Nov 3, 2014

Ms. No.: ER-14-721

Title: Silver Nanoparticles Affect on Gene Expression of Inflammatory and Neurodegenerative Responses in Mouse Brain Neural Cells

Journal: Environmental Research

Dear Editors and Reviewers,

We truly appreciate the opportunity given to us to revise our manuscript and prospect of having our paper published in *Environmental Research*.

In this version, we labeled the Figure 1, 4 and 5 according to reviewer's suggestion, and carefully organized the paragraphs and added the subtitles to point out the finding views in Discussion. To facilitate the review process, we highlighted our changes in yellow in the revised version of the manuscript.

Below please find our point-by-point to each comment/suggestion by the reviewers. If you have any questions, please contact me at cychuang@mx.nthu.edu.tw and thank you again for the careful and insightful review of our manuscript

Best Regards,

Chun-Yu Chuang

Associate professor

Department of Biomedicine Engineering and Environmental Sciences

National Tsing Hua University, Taiwan

E-mail: cychuang@mx.nthu.edu.tw

Tel.: +886 3-5715131 ext 34229;

Fax: +886-3-5733592

Date: Nov 3, 2014

Ms. No.: ER-14-721

Title: Silver Nanoparticles Affect on Gene Expression of Inflammatory and Neurodegenerative Responses in Mouse Brain Neural Cells

Journal: Environmental Research

Dear Editors and Reviewers,

We truly appreciate the opportunity given to us to revise our manuscript and prospect of having our paper published in *Environmental Research*.

In this version, we labeled the Figure 1, 4 and 5 according to reviewer's suggestion, and carefully organized the paragraphs and added the subtitles to point out the finding views in Discussion. To facilitate the review process, we highlighted our changes in yellow in the revised version of the manuscript.

Below please find our point-by-point to each comment/suggestion by the reviewers. If you have any questions, please contact me at cychuang@mx.nthu.edu.tw and thank you again for the careful and insightful review of our manuscript

Best Regards,

Chun-Yu Chuang

Associate professor

Department of Biomedicine Engineering and Environmental Sciences

National Tsing Hua University, Taiwan

E-mail: cychuang@mx.nthu.edu.tw

Tel.: +886 3-5715131 ext 34229;

Fax: +886-3-5733592

Reviewer #2:

(1) It is good for the authors to provide both 100 x and 400 x images in Figure 4 and 5. However, it needs to point out which area 400 x images are selected from 100 x ones. That is the typical way for the sound depiction of the images at different magnifications at the same time.

Response:

Thanks for your suggestion. In Figure 4 and 5, the white arrows pointed out the view of 400X images where are selected from 100X ones.

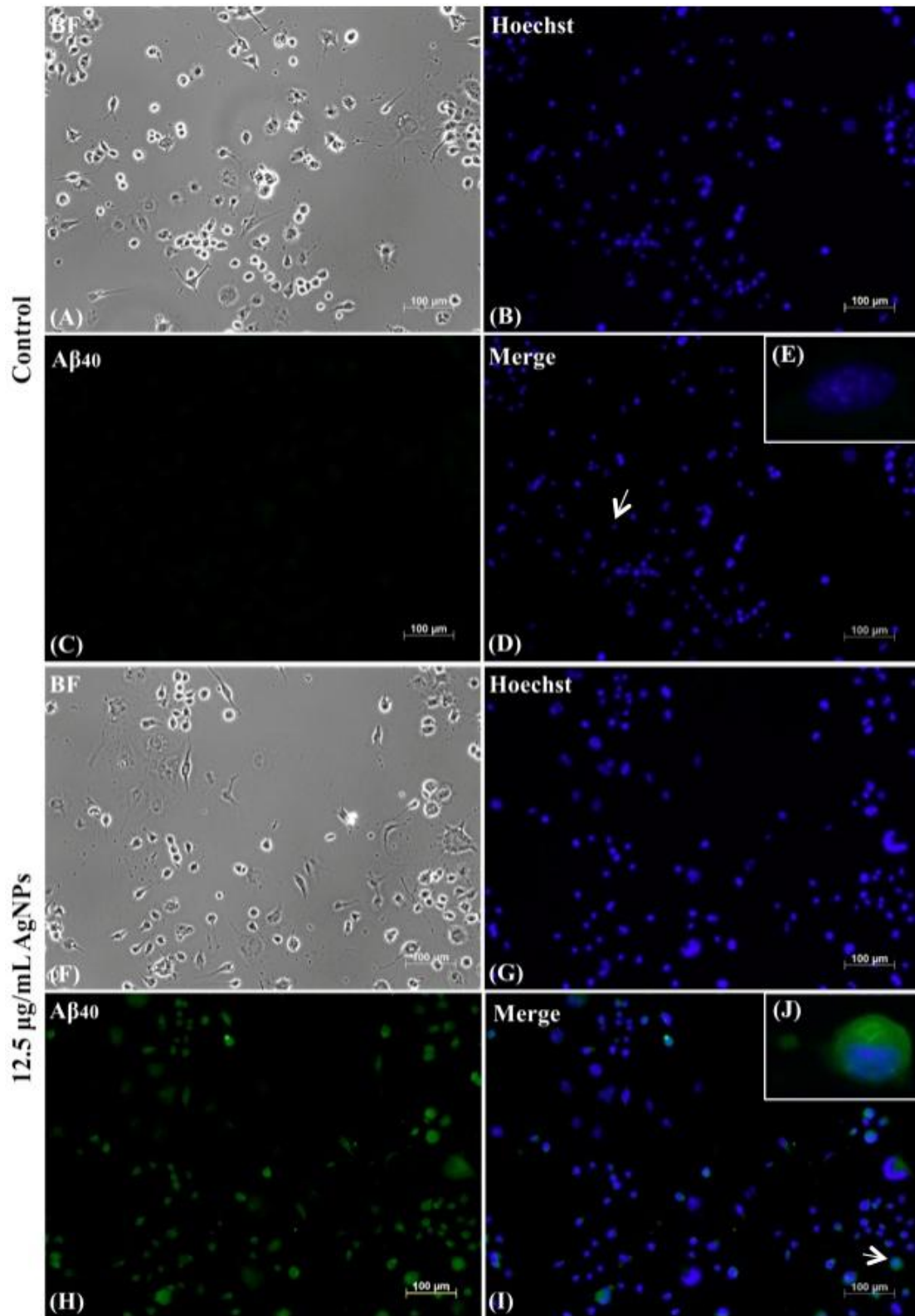


Fig. 4 Amyloid- β_{1-40} plaques inside mouse neuron N2a cells in exposure to AgNPs. Immunofluorescent detection of primary rabbit anti-mouse $A\beta_{1-40}$ was stained with secondary goat FITC-conjugated anti-rabbit IgG in N2a cells after 24 h 12.5 $\mu\text{g/ml}$ 3-5 nm AgNPs treatment. The control groups (A-D) and AgNPs exposure groups (F-I) were taken under 100X magnification respectively at 172 ms, 120 ms and 500 ms exposure time for bright field (BF), hoechst, and primary rabbit anti-mouse $A\beta_{1-40}$. (E) and (J) were a single cell image respectively according to (D) and (I) fields taken under 400X magnification. The white arrows pointed out the view of 400X images where are selected from 100X ones.

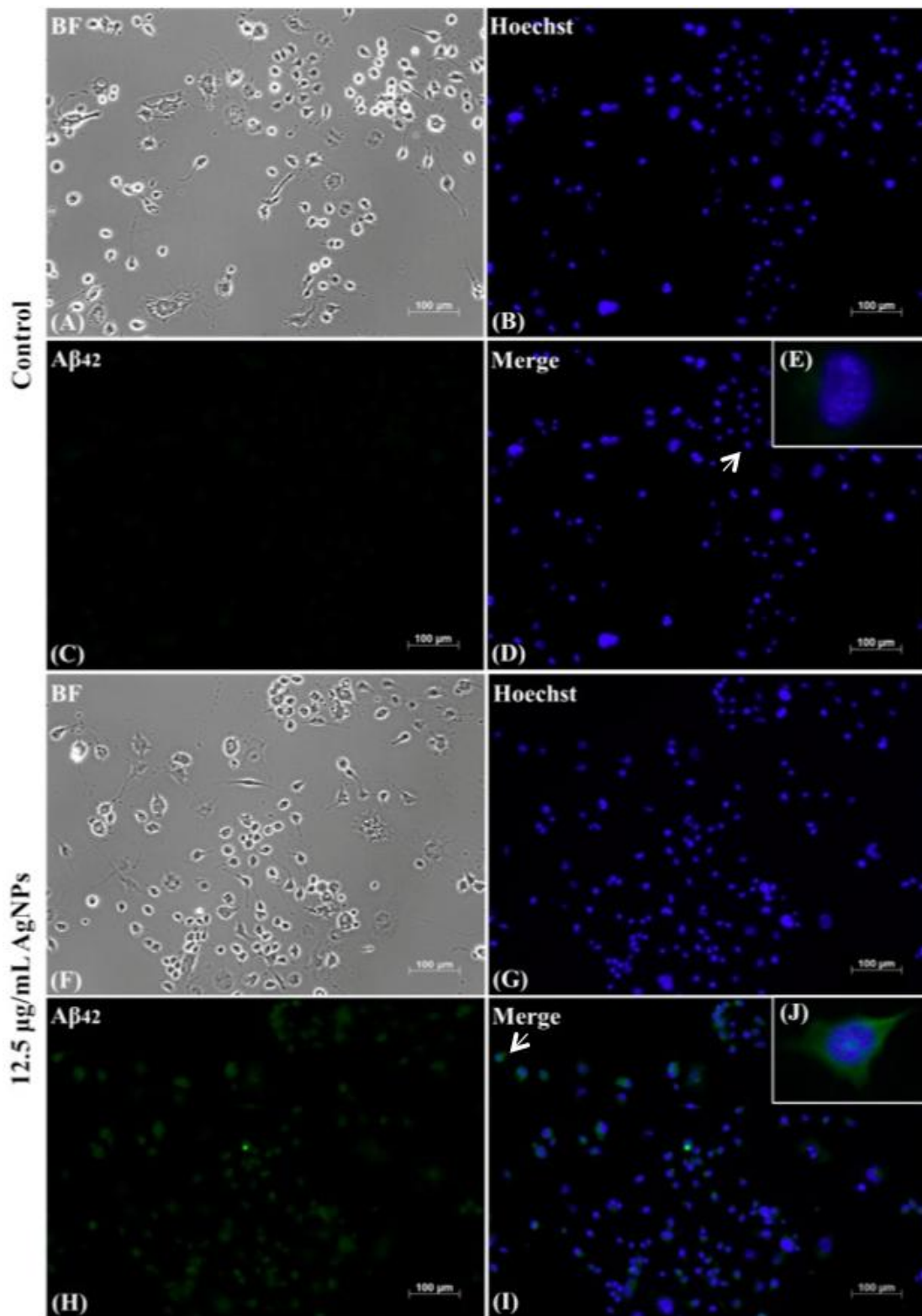


Fig. 5 Amyloid- β_{1-42} plaques inside mouse neuron N2a cells in exposure to AgNPs. Immunofluorescent detection of primary rabbit anti-mouse $A\beta_{1-42}$ was stained with secondary goat FITC-conjugated anti-rabbit IgG in N2a cells after 24 h 12.5 $\mu\text{g/ml}$ 3-5 nm AgNPs treatment. The control groups (A-D) and AgNPs exposure groups (F-I) were taken under 100X magnification respectively at 172 ms, 120 ms and 500 ms exposure time for bright field (BF), hoechst, and primary rabbit anti-mouse $A\beta_{1-42}$. (E) and (J) were a single cell image respectively according to (D) and (I) fields taken under 400X magnification. The white arrows pointed out the view of 400X images where are selected from 100X ones.

(2) For better visual comparison, Figure 1a and b are suggested to be revised. The authors may use cell lines as the category on the X-coordinate, while exposure doses can be depicted in the figure legends.

Response:

Thanks for your suggestion. We have labeled the category on the X- and Y-coordinate.

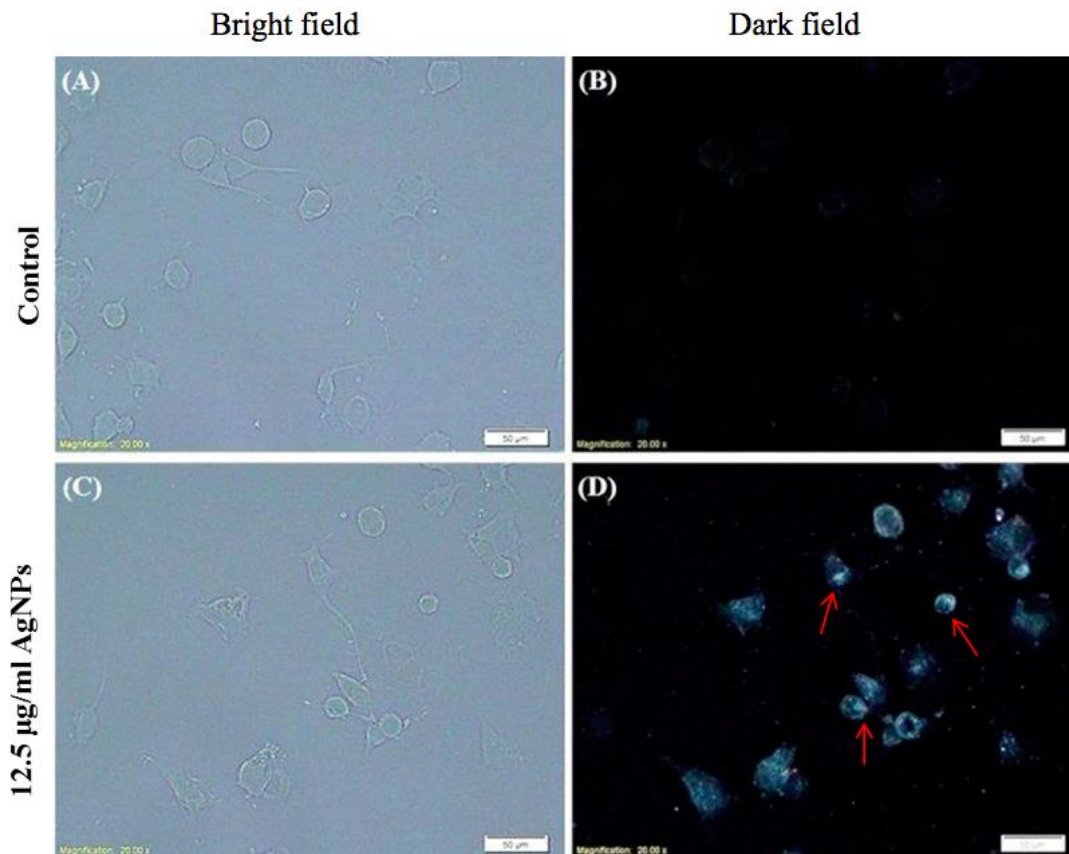


Fig. 1 AgNPs uptake in mouse neuron N2a cells. A polarizing microscope was used to detect 5 nm AgNPs distribution in N2a cells. N2a cells were (A, B) cultured in normal culture medium, or (C, D) exposed to 12.5 µg/ml AgNPs for 24 h. The bright field (A, C) and the dark field (B, D) indicate phase contrast image and polarizing image of corresponding cells respectively undertaken in 200X magnification with 30 us and 10 ms exposure time. The red arrows point the location of AgNPs reflecting the bright spots mainly located inside the neural cells.

(3) The discussion section is not well organized. More clear view needs to be elucidated in each paragraph

Response:

Thanks for your suggestion. We have organized the description in paragraphs, and added the subtitle to precisely point out the finding views for each paragraph.

Highlights

AgNPs can cross the cell membrane of mouse neuron cells.

AgNPs increased IL-1 β , CXCL13, MARCO and GSS for inflammation and oxidative stress.

AgNPs caused A β plaques deposition in neuron cells.

AgNPs induced APP, and reduced NEP and LDLR for A β plaque deposition.

It's necessary to take notice of AgNPs effect on neurodegenerative disorders.

Silver nanoparticles affect on gene expression of inflammatory and neurodegenerative responses in mouse brain neural cells

Chin-Lin Huang, I-Lun Hsiao, Ho-Chen Lin, Chu-Fang Wang, Yuh-Jeen Huang*, Chun-Yu Chuang*

Department of Biomedical Engineering and Environmental Sciences, National Tsing Hua University, Hsinchu, Taiwan

*Corresponding Author:

Chun-Yu Chuang

Department of Biomedical Engineering and Environmental Sciences

National Tsing Hua University

101, section 2, Kuang-Fu Road, Hsinchu 30013, Taiwan.

E-mail: cychuang@mx.nthu.edu.tw

Phone: +886-3-5715131 ext 34229

Fax: +886-3-5718649

Yuh-Jeen Huang

Department of Biomedical Engineering and Environmental Sciences

National Tsing Hua University

101, section 2, Kuang-Fu Road, Hsinchu 30013, Taiwan.

email: yjhuang@mx.nthu.edu.tw

Phone: +886-3-5715131 ext 35496

Fax: +886-3-5718649

E-mail: yjhuang@mx.nthu.edu.tw

Abstract

Silver nanoparticles (AgNPs) have antibacterial characteristics, and currently are applied in Ag-containing products. This study found neural cells can uptake 3-5 nm AgNPs, and investigated the potential effects of AgNPs on gene expression of inflammation and neurodegenerative disorder in murine brain ALT astrocytes, microglial BV-2 cells and neuron N2a cells. After AgNPs (5, 10, 12.5 µg/ml) exposure, these neural cells had obviously increased IL-1 β secretion, and induced gene expression of C-X-C motif chemokine 13 (*CXCL13*), macrophage receptor with collagenous structure (*MARCO*) and glutathione synthetase (*GSS*) for inflammatory response and oxidative stress neutralization. Additionally, this study found amyloid- β (A β) plaques for pathological feature of Alzheimer's disease (AD) deposited in neural cells after AgNPs treatment. After AgNPs exposure, the gene expression of amyloid precursor protein (*APP*) was induced, and otherwise, neprilysin (*NEP*) and low-density lipoprotein receptor (*LDLR*) were reduced in neural cells as well as protein level. These results suggested AgNPs could alter gene and protein expressions of A β deposition potentially to induce AD progress in neural cells. It's necessary to take notice of AgNPs distribution in the environment.

Keywords: silver nanoparticle; inflammation; gene expression; neurodegenerative disorder; Alzheimer's disease

1. Introduction

In recent years, nanotechnology grows rapidly, and nanoparticles are produced and widely utilized in diverse areas of different industrial applications because of its high interfacial reactivity and unique physicochemical properties (Loo et al., 2013). As to antibacterial / antifungal characteristics, silver nanoparticles (AgNPs) have been used in clothes, cosmetics, wound dressing, air-freshener sprays, water disinfectant, sunscreens, hygiene products and food containers, which increases the release of nanoparticles to environment and may cause exposure to human (Ribeiro et al., 2013). The exposure route for AgNPs happens via ingestion, inhalation or dermal contact. Kulthong et al. (2010) indicated that the antibacterial fabric from six commercial fabrics releases silver of AgNPs when is immersed in artificial sweat as a model to represent the human skin environment. In addition, AgNPs may have an access to systemic circulation through broken skin when we use the AgNP-containing products such as bandages or wound dressings (Singh and Ramarao, 2012). After injection different particles size of Ag (nanosized and microsized) in rats (62.8 mg/kg), AgNPs can translocate to the blood circulation and distribute throughout the main organs, especially in the kidney, liver, spleen, lung and brain, and induce blood-brain barrier (BBB) destruction and astrocyte swelling to cause neuronal degeneration (Tang et al., 2009).

Ag is one of the most toxic metals for the marine systems (Tappin et al., 2010), and the monovalent silver ion is considered as the most toxic silver species in aquatic systems and causes intracellular accumulation in phytoplankton (Lee et al., 2005).

However, the AgNPs (<100 nm, 0.5 and 1 ug/ml) cause nuclear condensation and induce higher dramatically cytotoxicity than Ag ions in human lymphoma cells (Eom and Choi, 2010). In addition, a proteomic analysis showed that 20 nm AgNPs interfere with protein regulations of mitochondrial translation, RNA processing, tRNA metabolism and cell proliferation more than Ag ions and larger size AgNPs (100 nm) in human colon adenocarcinoma LoVo cells (Verano-Braga et al., 2014). The diameter 139±37 nm AgNPs trigger dose-dependent effect of decreased cell viability on human lung carcinoma A549 cells in exposure to 5, 10 and 15 ug/ml AgNPs (Foldbjerg et al., 2011). Besides, the cell deaths in apoptosis and necrosis all increase after exposure to AgNPs (2.5, 5, 10 and 15 µg/ml). Moreover, Gaiser et al. (2013) pointed that 20 nm diameter nanoparticles can cause toxicity, inflammation and oxidative stress after exposure to human C3A hepatocytes and female Wistar rats. Besides, the inflammatory cytokines, e.g., IL-8, MIP2, IL-1RI and TNF-α, are both increased on *in vitro* and *in vivo* models after AgNPs-induction. Overall, the Ag and Cu nanoparticles can easily enter the mice brain to disrupt BBB permeability and induce neurotoxicity, which alters brain sensory, motor and cognitive functions (Sharma and Sharma, 2012). AgNPs (20 nm; 1, 5, 10 and 50 µg/ml) can reduce cell viability in primary rat cortical cells, and inhibit the sprouting of neuronal branches and elongation of neuritis for fragmentation and degeneration of mature neurons (Xu et al., 2013).

Brain is composed of endothelial cells, neurons and glial cells. Astrocytes are known as reactive astrogliosis cells to regulate metal homeostasis, supply nutrients to neurons and protect other brain cells against oxidative stress and metal toxicity (Sofroniew and

Vinters, 2010). Microglia are a type of glial cell major brain-resident macrophage-like cells in the central nerve system (CNS) to defend against microorganism invasion and injury, and release some cytokine factors to mediate neuroinflammatory processes (Wang et al., 2011). The inflammatory response, a tissue reaction to injury or an antigen, releases cytokines, chemokines, reactive oxygen species (ROS) and nitric oxides (NO) (Wei et al., 2013). Nerve cells connect to each other to form neural networks. Neurons are electrically excitable brain endothelium to transmit information through electrical and chemical signals via synapses and contact with perivascular astrocytes and pericytes (Weiss et al., 2009). Tang et al. (2010) indicated that AgNPs can cross through the BBB of rat brain to influence brain cells through transcytosis of capillary endothelial cells detectable by transmission electronic microscopy (TEM) and inductively-coupled plasma mass spectrometry (ICP-MS). Thus, the highest concentration of silver is observed in the kidneys and brain 28 days after injection a dose 5 mg kg⁻¹ bw AgNPs (20 and 200 nm) in Wistar rats (Dziendzikowska et al., 2012). Haase et al. (2012) found that AgNPs increase ROS generation and heme oxygenase 1 (HO-1) protein expression to cause neuronal oxidative damage and directly interfere with calcium responses in primary mixed neural cells. Increased levels of ROS occurred chronically in the early disease, which is relevant to neurodegenerative disorders, such as Alzheimer's and Parkinson's disease (Smith and Cass, 2007). Moreover, glutathione metabolism plays an important role of protecting cell from oxidative stress, and their gene expression related to oxidative stress are significantly altered in the caudate, frontal cortex and hippocampus of male C57BL/6N

mice after administered 25 nm AgNPs (Rahman et al., 2009).

The C-X-C motif chemokine 13 (*CXCL13*) play a role in the B-cell recruitment and distribution, associated with chronic inflammatory process (Nakajima et al., 2008). Macrophage receptor with collagenous structure (*MARCO*) is important for immune responses to bacterial infections by mediating the binding and phagocytosis of pathogens (Komine et al., 2013). Accordingly, studies have indicated that AgNPs can induce ROS and cytokines increasing and then cause inflammatory response. As *CXCL13* and *MARCO* genes are immune mediators in response to inflammation, exposure to AgNPs may change their gene expression. Moreover, glutathione synthetase (*GSS*) can synthesize glutathione (GSH) potentially to inhibit oxidative stress and prevent cellular damage from free radicals and peroxides (Koike et al., 2013), and AgNPs exposure probably alters *GSS* gene expression.

Amyloid beta ($A\beta$) is a peptide of amino acids that is processed from amyloid precursor protein (APP). $A\beta$ protein is considered the main responsible for neurodegenerative disorder such as Alzheimer's disease (AD). The up-regulation of *APP* gene expression interferes with $A\beta$ metabolism underlying the pathogenesis of AD (Dong et al., 2012). Low-density lipoprotein receptor (*LDLR*) enhances $A\beta$ uptake and degradation through binding $A\beta$ and $A\beta$ / ApoE complex (Basak et al., 2012). Thus, the down-regulation of *LDLR* gene leads $A\beta$ deposition. Besides, neprilysin (NEP) is a major $A\beta$ -degrading enzyme in brain to degrade $A\beta$ protein (El-Amouri et al., 2007). Sequentially, it is important to investigate the receptors and gene expression regulating $A\beta$ amyloid internalization in neural cells for understanding the AD pathogenesis.

According to previous studies, the information until now is not well known that whether the AgNPs-induced neuroinflammation cause the changes in gene expression related neurodegenerative disorder such as AD. In this study, we investigated whether the 3-5 nm AgNPs can pass through mouse brain neuronal cells and induce A β amyloid generation underlying the potential effect of AgNPs on gene expression of inflammatory response, oxidative stress, and A β deposition.

2. Material and methods

2.1 Cell culture and exposure

This study used three types of neural cells, murine brain ALT astrocytes (BCRC 60581), murine microglial BV-2 cells (ICLC ATL03001) and mouse neuroblastoma Neuro-2a (N2a) cells (BCRC 60026). N2a cells were cultured in high glucose Dulbecco's Modified Eagle's Medium (DMEM; CORNING, New York) supplemented with 10 percent fetal bovine serum (Invitrogen, Carlsbad, Canada), 1 percent antibiotic (Biowest, Loire Valley, France), 1 percent L-glutamine (Invitrogen), 1 percent sodium pyruvate (Invitrogen) in a cell incubator with 5 percent CO₂ at 37 °C. ALT cells and BV-2 cells were cultured in the similar medium with N2a cells except for the lack of 1 percent sodium pyruvate. When N2a cells grew to 70-80 percent confluence of a culture plate, the growth medium was removed and replaced with differentiation medium for two days. The Differentiation medium containing forskolin and isobutylmethylxanthine (IBMX) was added to N2a cells for 24 h differentiation. N2a cells can be differentiated into a neuron-like morphology with expression of several

neuronal markers. The 3-5 nm AgNPs were produced by a physical method without surfactants or stabilizers (Gold Nanotech Inc., Taiwan). AgNPs (0.5, 1, 5, 10 and 12.5 $\mu\text{g/ml}$) and lipopolysaccharides (LPS; 0.2 and 2 $\mu\text{g/ml}$; Invitrogen) were respectively added into the medium to treat ALT, BV-2 and N2a cells for 24 h exposure.

2.2 Polarizing microscope

N2a cells were cultured on glass coverslips with the treatment of AgNPs (5 nm, 12.5 $\mu\text{g/ml}$) for 24 h. After treatment, the cells on coverslips were fixed in 4 percent paraformaldehyde (PFA) for 10 min at 4°C, then washed with phosphate buffered saline (PBS) and mounted with slides in mounting medium. Images of AgNPs location were captured under the polarizing microscopy (IX71, Olympus, Tokyo, Japan).

2.3 Cell proliferation of neural cells

The neural cells $1 \times 10^4 \text{ cm}^{-2}$ were seeded in 96-well plates for cell viability analysis. After exposure to AgNPs or LPS, the suspensions were discarded, alamarBlue® reagent (DMEM / 10 percent FBS 1:10; Invitrogen) was added as a cell viability indicator followed by a 2 h incubation at 37°C, and the absorbance was monitored at 570 nm using 600 nm as a reference wavelength. The cell viability was calculated as $[\text{cell number of exposure samples}] / [\text{cell number of control}] \times 100$. Cell numbers were derived from a standard curve, which was obtained after seeding serially diluted cells (from 5×10^4 to 1.56×10^3 cells/ml) in a 96-well plate.

2.4 Cytokine assay of IL-1 β

The concentrations of pro-inflammatory cytokine IL-1 β were determined using ELISA kits (Mouse IL-1 β Instant ELISA, eBioscience, San Diego, Canada) according to the operation manual. A 96-well plate was coated with capture antibody (purified anti-mouse IL-1 β) in coating buffer and incubated overnight at 4°C. After three time wash with PBST (PBS with 1 percent Tween 20), the blocking solution (200 μ l) was added to each well with 1 h. After wash, the samples (100 μ l) and IL-1 β standards (16-2000 pg/ml) were added to each well for 2 h incubation at room temperature. After incubation and wash, the 100 μ l of biotin-conjugated anti-mouse IL-1 β and streptavidin-horseradish peroxidase (HRP) were added to each well for 30 min incubation, then wash, and each well was added to 100 μ l TMB (3,3',5,5'-Tetramethylbenzidine) substrate solution for 15 min. Final, the 50 μ l stop solution (2 M H₂SO₄) was added to each well and the optical density was determined at 450 nm using a VERSAmax microplate reader (Molecular Devices, Sunnyvale, Canada).

2.5 Immunofluorescent detection of A β protein

N2a cells cultured on coverslips were washed twice with 1X PBS and then fixed with 4 percent PFA for 10 min at 4°C, and washed with PBS. Cells were permeabilized with 0.1 percent Triton X-100 / PBS solution at room temperature for 30 min, blocked in 2 percent horse serum (HS) at room temperature for 30 min, and then incubated for 1 h respectively with primary rabbit anti-mouse A β ₁₋₄₀ (1:500; Cat. 171608, Merck

Millipore, Darmstadt, Germany) or primary rabbit anti-mouse A β ₁₋₄₂ (1:500; Cat. 171609, Merck Millipore). The coverslips were then washed three times with PBS and stained with secondary fluorescein isothiocyanate (FITC)-conjugated goat anti-rabbit IgG (1:500; Cat. 12-507, Merck Millipore). After washed in PBS, the coverslips were incubated with Hoechst 33258 (1:20; Cat. 23491-45-4, Sigma-Aldrich, St. Louis, MO) and rinsed in PBS. Coverslips were mounted on slides in mounting medium. Immunofluorescence images were captured with an inverted microscope with fluorescence filters (Axio Observer A1/D1, Zeiss, Oberkochen, Germany).

2.6 RNA extraction

Total RNA was isolated respectively from ALT, BV-2 and N2a cells in exposure to AgNPs after 24 h using RNA Trizol (Invitrogen). After the culture medium were removed, neural cells were dissolved in 1 ml of TRIZOL reagent, and then 0.2 ml chloroform was added a 1.5 ml eppendorf tube. The mixture was shook vigorously for 15 s and centrifuged at 12,000 g for 15 min at 4°C. Next, the supernatant was transferred to a fresh tube, and 0.5 ml isopropanol (SIGMA) was added at room temperature for 10 min. The RNA was precipitated after centrifugation at 12,000 g for 10 min at 4°C. The RNA pellet was washed with 1 ml of 75 percent ethanol (Taiwan Tobacco & Liquor Corporation, Taipei, Taiwan) and centrifuged at 7500 g for 5 min at 4°C to remove the ethanol. The RNA pellet was dried up and diluted with RNase-free water. The purified RNA was quantified using Nanodrop 2000c (Thermo, Wilmington, Massachusetts).

2.7 Reverse transcription polymerase chain reaction (RT-PCR)

cDNA was synthesized from total RNA by a high-capacity cDNA reverse transcription kit (Applied Biosystems, California). The 3 µg RNA was added 1.0 µl MultiScribe™ reverse transcriptase (50 unit µl⁻¹), 2.0 µl 10X RT random primers, 0.8 µl 20X concentrated dNTP mix, 2.0 µl 10X concentrated RT buffer and RNase free water (DEPC water) in a 0.2 ml PCR tube, and subsequently amplified by PCR with one cycle of 20°C 10 min, 37°C 120 min and 85°C 5 s.

2.8 Real time PCR for gene expression quantitation

One hundred nanograms cDNA was amplified by PCR with 40 cycles of denaturing (95°C, 15 s), annealing (55°C, 30 s) and extension (72°C, 45 s) using 2X power SYBR green PCR master mix (Applied Biosystems). PCR primers: *CXCL13* sense 5'-ATG TGT GAA TCC TCG TGC CAA-3' and anti-sense 5'-AAA AAA GGT GCA GGT GTG TCT-3'; *MARCO* sense 5'-GGG TCA AAA AGG CGA ATC T-3' and anti-sense 5'-ATG TTC CCA GAG CCA CCT-3'; *GSS* sense 5'-GGT ATC TTC CCT CAG CAG CCT T-3' and anti-sense 5'-GCT TCC ATT CCC ACA CTC CAA A-3'; *APP* sense 5'-CTG GAC GGT TCG GGC TCT-3' and anti-sense 5'-CGG GTC TGA CTC CCA CTT TC-3'; *LDLR* sense 5'-TCC AAT CAA TTC AGC TGT GGA G-3' and anti-sense 5'-ATC AGA GCC ATC TAG GCA ATC TCG-3'; *NEP* sense 5'-AAA GCC AAA GAA GAA ACA GCG A-3' and anti-sense 5'-GCA TAG AGA GCG ATC ATT GTC ACC G-3'; *β-actin* sense 5'-ATG CTC CCC GGG CTG TAT-3'

and anti-sense 5'-CCA CTG CTC CGG GTC TCG-3'. Quantitative analysis of PCR products was carried out by a sequence detector (Model 7300, Applied Biosystems) according to the manufacturer's instruction. The signal of SYBR green was measured at 530 nm during extension phase, and collected and analyzed with SDS 1.0 software. The threshold cycle (Ct) value denotes the cycle number at which the fluorescence generated within a reaction across the threshold, thus the Ct value is at the point accumulated a sufficient number of amplicons during the reaction. The relative level of mRNA expression is a ratio of optical density of the experimental groups to that of *β-actin* (internal control, an endogenous house-keeping gene). The relative Ct value of different condition was compared to that of control cells as reference to estimate the fold change of mRNA expression among the samples. Triplicates were performed for each primer pair.

2.9 Western blotting for protein determination

N2a cells were lysed with RIPA buffer (Cell Signaling, Danvers, MA) containing proteinase inhibitor Cocktail (Sigma), and centrifuged at 8,000 g for 3 min at 4°C. Protein samples in the supernatant were immediately transferred, and the concentration was measured using a Bicinchoninic Acid Protein Assay Kit (Sigma). Protein in the samples were then electrophoresed over a 10% sodium dodecyl sulfate polyacrylamide gel, and subsequently transferred to a hydrophobic PVDF membrane (Millipore). The membrane-bound proteins were respectively immunostained with 1:1000 primary rabbit anti-mouse NEP (CD10) (Cat. EPR 2997, Abcam, Cambridge, MA), APP (Cat.

EPR 5118-34, Abcam), LDLR (Cat. EP 155311, Abcam) or β -actin (Senta Cruz Biotechnology, Senta Cruz, CA) antibody and followed by treatment with secondary anti-rabbit IgG horse radish peroxidase (HRP) antibody (Senta Cruz Biotechnology, CA). The tagged proteins were detected using a chemiluminescence reagent (Thermo Scientific, Rockford, IL) and photographed in a G:Box ChemiXT 16 system (Syngene, Frederick, MD). The band intensities in the western blots were quantified by ImageJ software.

2.10 Statistical analysis

Results were described as mean \pm standard deviation. Data analysis was conducted by the statistical package SPSS 13.0 (SPSS Inc., Chicago, Illinois). The statistically significant differences of cell proliferation, IL-1 β , gene expression and protein respectively between AgNPs treatment and control were analyzed using Student's *t* test.

All statistical significances were determined at two-tailed *p* value < 0.05 .

3. Results

3.1 Permeability, cytotoxicity and pro-inflammation of AgNPs in neural cells

The zeta potential of the 3-5 nm AgNPs used in this study was -4.2 mV in culture medium. The 3-5 nm AgNPs (12.5 $\mu\text{g/ml}$) can cross the cell membrane of N2a cells detectable under polarizing microscope (Fig. 1). The cell proliferation of ALT, BV-2 and N2a cells exposed to AgNPs (0.5, 1, 5, 10 and 12.5 $\mu\text{g/ml}$) and LPS (0.2, 2 $\mu\text{g/ml}$) for 24 h were shown in Fig. 2. The cell proliferation was decreased in ALT cells (0.5, 1, 10 and 12.5 $\mu\text{g/ml}$) and N2a cells (12.5 $\mu\text{g/ml}$) but not differently changed in BV-2 cells after AgNPs exposure. LPS decreased cell proliferation obviously in ALT cells (2 $\mu\text{g/ml}$) and BV-2 cells (0.2 $\mu\text{g/ml}$). Additionally, the IL-1 β secretion of ALT, BV-2 and N2a cells was detected after 24 h AgNPs exposure (Fig. 3). IL-1 β protein was significantly increased in BV-2 cells after 12.5 $\mu\text{g/ml}$ AgNPs exposure.

3.2 A β amyloid deposition in neural cells after AgNPs exposure

The immunofluorescence images revealed that A β_{1-40} (Fig. 4) and A β_{1-42} (Fig. 5) proteins were inducible to generate after AgNPs exposure 12.5 $\mu\text{g/ml}$ in N2a cells, and detectable in a fluorescence microscope.

3.3 Gene expression of neural cells in exposure to AgNPs

LPS induced the expression of *CXCL13* and *MARCO* genes for inflammatory process and phagocytosis. The gene expression of *CXCL13* and *MARCO* were increased in ALT, BV-2 and N2a cells at the higher dose of AgNPs (5, 10 and 12.5

$\mu\text{g/ml}$) (Fig. 6A and 6B). The *GSS* mRNA level was significantly decreased in ALT cells (0.5, 1, 5, 10 and 12.5 $\mu\text{g/ml}$) and increased in BV-2 cells (10 and 12.5 $\mu\text{g/ml}$) after AgNPs exposure (Fig. 6C). On the other hand, the gene expression of AD process related genes such as *APP*, *LDLR* and *NEP* were also altered in exposure to AgNPs. The gene expression of *APP* was elevated in ALT, BV-2 (5, 10 and 12.5 $\mu\text{g/ml}$) and N2a (12.5 $\mu\text{g/ml}$) cells (Fig. 6D). On the contrary, the decreased *LDLR* mRNA level was observed in 12.5 $\mu\text{g/ml}$ AgNPs-treated ALT, BV-2 and N2a cells (Fig. 6E). *NEP* gene expression also reduced significantly in N2a cells exposed to AgNPs (Fig. 6F).

3.4 Protein determination of neural cells in exposure to AgNPs

The protein levels of APP, LDLR and NEP were determined after N2a cells exposed to 1, 5, 10, 12.5 and 15 $\mu\text{g/ml}$ AgNPs, respectively. APP levels were obviously induced in exposure to 10, 12.5 and 15 $\mu\text{g/ml}$ AgNPs (Fig. 7A). LDLR levels were significantly reduced after exposure to 1, 10 and 15 $\mu\text{g/ml}$ AgNPs (Fig. 7B). The level of NEP protein was increased after AgNPs and returned to the steady state as control group (Fig. 7C).

4. Discussion

This study found that 3-5 nm AgNPs can cross the cell membrane (Fig. 1), induced IL-1 β secretion for inflammatory response (Fig. 3), and accelerate A β 1-40 (Fig. 4) and A β 1-42 (Fig. 5) generation and deposition. AgNPs exposure (5, 10, 12.5 $\mu\text{g/ml}$) induced the gene expression of *CXCL13*, *MARCO* and *GSS* for inflammatory response

and oxidative stress (Fig. 6). Besides, AgNPs exposure increased the gene expression and protein level of APP for A β generation, and reduced LDLR and NEP for A β uptake/transporter and A β degradation (Fig. 6 and Fig. 7). These findings suggested that AgNPs exposure potentially caused neurodegenerative disorder progression underlying A β deposition.

4.1 AgNPs exposure induced inflammatory response in mouse neural cells

This study found that AgNPs crossed the cell membrane of neuron cells and mostly distributed in the cytoplasm (Fig. 1), and induced IL-1 β secretion (Fig. 3) for inflammatory response in neural cells (astrocytes, microglia and neuron cells). AgNPs and iron oxide nanoparticles in astrocytes are internalized by endocytotic uptake processes into cellular vesicles to respectively release Ag and ferrous iron and induce ROS generation and inflammation (Hohnholt et al., 2013). Prasad et al. (2013) indicated that AgNPs have a higher rate of cellular uptake compared with AgNO₃ and cause oxidative stress and inflammatory response in liver HepG2 cells. Moreover, AgNPs can enter the brain through the olfactory nerve, and the toxic effect of AgNPs is stronger than silver ions because ions are consumed before reaching the cell membrane (Wijnhoven et al., 2009, Quadros and Marr, 2010). Besides, in the analysis of Mouse Oxidative Stress and Antioxidant Defense Arrays, male C57BL/6N mice administered with 25 nm AgNPs change the expression of oxidative stress associated genes in the caudate, frontal cortex and hippocampus (Rahman et al., 2009).

The results of this study indicated that AgNPs activated stress-responsive gene *GSS*

and immune reaction genes *CXCL13* and *MARCO*. AgNPs induces inflammatory cytokine TNF- α release, ROS and endoplasmatic reticulum (ER) stress response in zebrafish liver cells (Christen et al., 2013). Cha et al. (2008) found the AgNPs-treated liver cells have the up-regulated gene expression of *CXCL13* and *MARCO* to induce apoptosis and inflammation. Moreover, chemokine C-C motif ligand (CCL) 2 can activate resident microglias in the brain to recruit peripheral macrophages and increase chemokine family *CCL24* gene expression (Selenica et al., 2013). Kang et al. (2012) reported that 7.5 ± 2.5 nm AgNPs evoke ROS generation and increase a major cellular thiol antioxidant GSH level in human renal proximal tubular epithelial HK-2 cells. Importantly, the diameter of 20 and 40 nm AgNPs (10 and 20 $\mu\text{g}/\text{ml}$) can lead to mixed primary cortical neural cells increase the level of ROS in accompanied with calcium rises, and the smaller AgNPs have stronger cytotoxicity than bigger ones (Haase et al., 2012).

4.2 AgNPs exposure changed gene expression and protein level of amyloid plaque deposition in mouse neuron cells

Neuroinflammation and beta-amyloid deposition led to memory impairment in Alzheimer's disease transgenic mice (Xu et al., 2014). According to above studies, we inferred that chronic ROS increase and unbalance calcium level in neural cells may cause AD neurodegenerative disorder. This study observed that AgNPs caused A β amyloid plaque deposition in mouse neuron N2a cells (Fig. 4 and Fig. 5). Furthermore, this study determined the gene expression corresponding to A β generation and

deposition in neural cells treated with AgNPs (Fig. 6).

The ability of insoluble 40 to 42 peptides of A β amyloid has been considered more rapidly aggregation and more neurotoxicity in AD progression (Landau et al., 2013). In this study, AgNPs exposure can induce A β ₁₋₄₀ and A β ₁₋₄₂ peptides aggregation in neural cells (Fig. 4 and Fig. 5). Additionally, the gene expression (Fig. 6) and protein level (Fig. 7) of A β amyloid generation and deposition relevant to AD progression have been explored after AgNPs exposure. AgNPs induced the expression of *APP*, and otherwise, attenuated *NEP* and *LDLR* for the potential effect on A β deposition. APP protein is an integral membrane glycoprotein expressing in the brain and central nervous system, and A β amyloid is produced by sequential cleavage of APP by β -secretase and γ -secretase (Dong et al., 2012). The increased APP and β -secretase levels lead to increase A β amyloid formation and aggregation potentially for neurodegenerative disease (Meraz-Rios et al., 2013). The results of this study suggested that AgNPs led to up-regulate the gene expression of *APP*, and down-regulate A β uptake gene *LDLR* and A β degradation gene *NEP*. LDLR can enhance A β uptake and degradation to regulate A β levels in the mouse brain (Basak et al., 2012). Cao et al. (2006) indicated that A β deposition accompanies with the increased ApoE expression in *LDLR*-deficient Tg2576 mice. *LDLR*-deficient Tg2576 mice have disorders in hypercholesterolemia, age-dependent cerebral β -amyloidosis and spatial learning deficits after A β deposition. Thus, LDLR plays an important role in amyloidosis and the development of Alzheimer-type learning impairment. NEP is the major protease involved in A β degradation. The decreased *NEP* mRNA level is observed in AD patients (Wang et al.,

2010). AD patients have the significantly lower *NEP* mRNA and protein levels in the brain with high A β plaque burdens (Park et al., 2013).

4.3 The potential mechanism of AD pathogenesis in mouse neural cells exposure to AgNPs

This study observed that AgNPs activated the gene expression of *GSS*, *CXCL13* and *MARCO* for stress-response and immune reaction, and induced *APP* and attenuated *NEP* and *LDLR* genes for the potential effect on A β deposition. Regarding to our findings in this study, a schematic diagram illustrated in Fig. 8 described that AgNPs exposure in brain neural cells results in gene expression changes underlying the possible progression of A β plaque deposition for AD pathological feature.

Inflammation elicits A β deposition via the activated microglia cells (Cameron and Landreth, 2010). This present study found AgNPs can enter into N2a cells and induce inflammatory response and A β deposition. The gene expression of *CXCL13*, *MARCO* and *GSS* in ALT, BV-2 and N2a cells are enhanced to defense against AgNPs-induced inflammatory reaction and oxidative stress. The APP protein is assembled from amino acids using information encoded in *APP* gene, which can be cleaved by α -secretase, β -secrease and γ -secrease to produce different length of A β peptides such as A β ₁₋₄₀ or A β ₁₋₄₂. Both of receptor for advanced glycation end product (RAGE) and low density lipoprotein receptor-related protein 1 (LRP1) are A β receptors able to bind A β or ApoE / A β complexes. RAGE transports A β proteins from blood to brain; in contrast, LRP1 transfers A β proteins from brain to blood (Kanekiyo et al., 2012, Han et al., 2011).

LDLR plays the main regulator with ApoE in CNS trafficking and breaking the balance of A β levels. The different isoforms of ApoE play different function, the neutral ApoE3 and protective ApoE2 can support A β transport or degradation, and the AD-risk factor ApoE4 accelerates A β aggregation for amyloid plaque formation (Morris et al., 2010). There are sequential pathways to balance the A β levels in the brain, e.g., A β clearance through BBB via RAGE and LRP1, A β degradation via NEP protease and insulin-degrading enzyme (IDE), and A β deposition internalized in neural cells via ApoE receptor when ApoE3 > ApoE4. AgNPs can activate *APP* gene to generate A β amyloid, and disturb ApoE transport and reduce *NEP* and *LDLR* expression to accelerate A β aggregation and deposition in neural cells.

5. Conclusion

In summary, this study identified 3-5 nm AgNPs can enter in mouse neural cells to induce pro-inflammatory cytokine secretion and increase A β amyloid deposition in response to the changes of gene expression in inflammatory response, oxidative stress and A β degradation. These results suggested that AgNPs-induced neuroinflammatory response and A β deposition might evolve the progress of neurodegenerative disorders.

It is necessary to note the daily usage of silver nanoparticles.

Acknowledgement

We thank Gold Nanotech, Inc., Taiwan for providing AgNP materials in this collaborative research.

Figure Legends

Fig. 1 AgNPs uptake in mouse neuron N2a cells. A polarizing microscope was used to detect 5 nm AgNPs distribution in N2a cells. N2a cells were (A, B) cultured in normal culture medium, or (C, D) exposed to 12.5 $\mu\text{g/ml}$ AgNPs for 24 h. The bright field (A, C) and the dark field (B, D) indicate phase contrast image and polarizing image of corresponding cells respectively undertaken in 200X magnification with 30 μs and 10 ms exposure time. The red arrows point the location of AgNPs reflecting the bright spots mainly located inside the neural cells.

Fig. 2 Cell proliferation after exposure to AgNPs and LPS. Neural cells were treated with different concentration of 3-5 nm AgNPs (0.5, 1, 5, 10 and 12.5 $\mu\text{g/ml}$) and LPS (ALT 2 $\mu\text{g/ml}$, BV-2 0.2 $\mu\text{g/ml}$ and N2a 2 $\mu\text{g/ml}$) for 24 h. The data were presented as mean \pm SD (n=3). *indicates significant difference at $p < 0.05$ compared with control.

ALT: astrocyte, BV-2: microglia, N2a: neuron cells.

Fig. 3 Cytokines IL-1 β in neural cells after exposure to AgNPs and LPS. (A) ALT, (B) BV-2 and (C) N2a cells were respectively treated with different concentration of 3-5 nm AgNPs (5 and 12.5 $\mu\text{g/ml}$) and LPS (ALT 2 $\mu\text{g/ml}$, BV-2 0.2 $\mu\text{g/ml}$ and N2a 2 $\mu\text{g/ml}$) for 24 h. The data were presented as mean \pm SD (n=3). *indicates significant difference at $p < 0.05$ compared with control. ALT: astrocyte, BV-2: microglia, N2a: neuron cells.

Fig. 4 Amyloid- β_{1-40} plaques inside mouse neuron N2a cells in exposure to AgNPs.

Immunofluorescent detection of primary rabbit anti-mouse $A\beta_{1-40}$ was stained with secondary goat FITC-conjugated anti-rabbit IgG in N2a cells after 24 h 12.5 $\mu\text{g/ml}$ 3-5 nm AgNPs treatment. The control groups (A-D) and AgNPs exposure groups (F-I) were taken under 100X magnification respectively at 172 ms, 120 ms and 500 ms exposure time for bright field (BF), hoechst, and primary rabbit anti-mouse $A\beta_{1-40}$. (E) and (J) were a single cell image respectively according to (D) and (I) fields taken under 400X magnification. The white arrows pointed out the view of 400X images where are selected from 100X ones.

Fig. 5 Amyloid- β_{1-42} plaques inside mouse neuron N2a cells in exposure to AgNPs.

Immunofluorescent detection of primary rabbit anti-mouse $A\beta_{1-42}$ was stained with secondary goat FITC-conjugated anti-rabbit IgG in N2a cells after 24 h 12.5 $\mu\text{g/ml}$ 3-5 nm AgNPs treatment. The control groups (A-D) and AgNPs exposure groups (F-I) were taken under 100X magnification respectively at 172 ms, 120 ms and 500 ms exposure time for bright field (BF), hoechst, and primary rabbit anti-mouse $A\beta_{1-42}$. (E) and (J) were a single cell image respectively according to (D) and (I) fields taken under 400X magnification. The white arrows pointed out the view of 400X images where are selected from 100X ones.

Fig. 6 Quantitative changes of (A) *CXCL13*, (B) *MARCO*, (C) *GSS*, (D) *APP*, (E) *LDLR* and (F) *NEP* gene expression in the neural cells with the treatment of 3-5 nm

AgNPs or LPS. Neural cells were treated with different concentration of 3-5 nm AgNPs (0.5, 1, 5, 10 and 12.5 $\mu\text{g/ml}$) and LPS (ALT 2 $\mu\text{g/ml}$, BV-2 0.2 $\mu\text{g/ml}$ and N2a 2 $\mu\text{g/ml}$) for 24 h. The data were presented as mean \pm SD (n=3). *indicates significant difference at $p < 0.05$ compared with control. ALT: astrocyte, BV-2: microglia, N2a: neuron cells.

Fig. 7 Protein levels of APP, LDLR and NEP in N2a cells after AgNPs exposure. The total protein were 40, 40 and 100 μg individually loaded for immunoblotting to determine (A) APP, (B) LDLR and (C) NEP in N2a cells exposed to 1, 5, 10, 12.5 and 15 $\mu\text{g/ml}$ AgNPs for 24 h, and quantified by ImageJ. *indicates significant difference at $p < 0.05$ compared with control.

Fig. 8 A schematic diagram of AgNPs exposure in brain neural cells to alter gene expression potentially resulting in the progression of A β plaque deposition and pathological feature of Alzheimer's disease. AgNPs can enter across neuronal cell membrane and induce the gene expression of *CXCL13*, *MARCO* and *GSS* in response to inflammatory reaction and oxidative stress. Sequentially, *APP* gene is activated for A β amyloid production, ApoE transport is influenced to accelerate A β aggregation, and *NEP* and *LDLR* genes are reduced for A β deposition. In addition, the A β proteins are increased through the up-regulated *RAGE* and down-regulated *LRP1* expression, and the dramatically enhanced level of A β proteins lead to decrease *IDE* and *NEP* gene expression to accelerate A β deposition. The AgNPs-induced neuroinflammatory

response and A β amyloid deposition might evolve neurodegenerative Alzheimer's disease. The number and arrow marked in red are fold-change levels and up-/down-regulation of gene expression.

References

- BASAK, J. M., VERGHESE, P. B., YOON, H., KIM, J. & HOLTZMAN, D. M. 2012. Low-density lipoprotein receptor represents an apolipoprotein E-independent pathway of Abeta uptake and degradation by astrocytes. *J Biol Chem*, 287, 13959-71.
- CAMERON, B. & LANDRETH, G. E. 2010. Inflammation, microglia, and Alzheimer's disease. *Neurobiol Dis*, 37, 503-9.
- CAO, D., FUKUCHI, K., WAN, H., KIM, H. & LI, L. 2006. Lack of LDL receptor aggravates learning deficits and amyloid deposits in Alzheimer transgenic mice. *Neurobiol Aging*, 27, 1632-43.
- CHA, K., HONG, H. W., CHOI, Y. G., LEE, M. J., PARK, J. H., CHAE, H. K., RYU, G. & MYUNG, H. 2008. Comparison of acute responses of mice livers to short-term exposure to nano-sized or micro-sized silver particles. *Biotechnol Lett*, 30, 1893-9.
- CHRISTEN, V., CAPELLE, M. & FENT, K. 2013. Silver nanoparticles induce endoplasmatic reticulum stress response in zebrafish. *Toxicol Appl Pharmacol*, 272, 519-28.
- DONG, S., DUAN, Y., HU, Y. & ZHAO, Z. 2012. Advances in the pathogenesis of Alzheimer's disease: a re-evaluation of amyloid cascade hypothesis. *Transl Neurodegener*, 1, 18.
- DZIENDZIKOWSKA, K., GROMADZKA-OSTROWSKA, J., LANKOFF, A., OCZKOWSKI, M., KRAWCZYNSKA, A., CHWASTOWSKA, J., SADOWSKA-BRATEK, M., CHAJDUK, E., WOJEWODZKA, M., DUSINSKA, M. & KRUSZEWSKI, M. 2012. Time-dependent biodistribution and excretion of silver nanoparticles in male Wistar rats. *J Appl Toxicol*, 32, 920-8.
- EL-AMOURI, S. S., ZHU, H., YU, J., GAGE, F. H., VERMA, I. M. & KINDY, M. S. 2007. Noprilysin protects neurons against Abeta peptide toxicity. *Brain Res*, 1152, 191-200.
- EOM, H. J. & CHOI, J. 2010. p38 MAPK activation, DNA damage, cell cycle arrest and apoptosis as mechanisms of toxicity of silver nanoparticles in Jurkat T cells. *Environ Sci Technol*, 44, 8337-42.
- FOLDBJERG, R., DANG, D. A. & AUTRUP, H. 2011. Cytotoxicity and genotoxicity of silver nanoparticles in the human lung cancer cell line, A549. *Arch Toxicol*, 85, 743-50.
- GAISER, B. K., HIRN, S., KERMANIZADEH, A., KANASE, N., FYTIANOS, K., WENK, A., HABERL, N., BRUNELLI, A., KREYLING, W. G. & STONE, V. 2013. Effects of silver nanoparticles on the liver and hepatocytes in vitro. *Toxicol Sci*, 131, 537-47.
- HAASE, A., ROTT, S., MANTION, A., GRAF, P., PLENDL, J., THUNEMANN, A. F., MEIER, W. P., TAUBERT, A., LUCH, A. & REISER, G. 2012. Effects of silver nanoparticles on primary mixed neural cell cultures: uptake, oxidative stress and acute calcium responses. *Toxicol Sci*, 126, 457-68.
- HAN, S. H., KIM, Y. H. & MOOK-JUNG, I. 2011. RAGE: the beneficial and deleterious effects by diverse mechanisms of actions. *Mol Cells*, 31, 91-7.
- HOHNHOLT, M. C., GEPPERT, M., LUTHER, E. M., PETTERS, C., BULCKE, F. & DRINGEN, R. 2013. Handling of iron oxide and silver nanoparticles by astrocytes. *Neurochem*

Res, 38, 227-39.

- KANEKIYO, T., LIU, C. C., SHINOHARA, M., LI, J. & BU, G. 2012. LRP1 in brain vascular smooth muscle cells mediates local clearance of Alzheimer's amyloid-beta. *J Neurosci*, 32, 16458-65.
- KANG, S. J., LEE, Y. J., LEE, E. K. & KWAK, M. K. 2012. Silver nanoparticles-mediated G2/M cycle arrest of renal epithelial cells is associated with NRF2-GSH signaling. *Toxicol Lett*, 211, 334-41.
- KOIKE, S., OGASAWARA, Y., SHIBUYA, N., KIMURA, H. & ISHII, K. 2013. Polysulfide exerts a protective effect against cytotoxicity caused by t-buthylhydroperoxide through Nrf2 signaling in neuroblastoma cells. *FEBS Lett*, 587, 3548-55.
- KOMINE, H., KUHN, L., MATSUSHITA, N., MULE, J. J. & PILON-THOMAS, S. 2013. Examination of MARCO activity on dendritic cell phenotype and function using a gene knockout mouse. *PLoS One*, 8, e67795.
- KULTHONG, K., SRISUNG, S., BOONPAVANITCHAKUL, K., KANGWANSUPAMONKON, W. & MANIRATANACHOTE, R. 2010. Determination of silver nanoparticle release from antibacterial fabrics into artificial sweat. *Part Fibre Toxicol*, 7, 8.
- LANDAU, S. M., LU, M., JOSHI, A. D., PONTECORVO, M., MINTUN, M. A., TROJANOWSKI, J. Q., SHAW, L. M., JAGUST, W. J. & ALZHEIMER'S DISEASE NEUROIMAGING, I. 2013. Comparing positron emission tomography imaging and cerebrospinal fluid measurements of beta-amyloid. *Ann Neurol*, 74, 826-36.
- LEE, D. Y., FORTIN, C. & CAMPBELL, P. G. 2005. Contrasting effects of chloride on the toxicity of silver to two green algae, *Pseudokirchneriella subcapitata* and *Chlamydomonas reinhardtii*. *Aquat Toxicol*, 75, 127-35.
- LOO, S. L., FANE, A. G., LIM, T. T., KRANTZ, W. B., LIANG, Y. N., LIU, X. & HU, X. 2013. Superabsorbent Cryogels Decorated with Silver Nanoparticles as a Novel Water Technology for Point-of-Use Disinfection. *Environ Sci Technol*, 47, 9363-71.
- MERAZ-RIOS, M. A., TORAL-RIOS, D., FRANCO-BOCANEGRA, D., VILLEDA-HERNANDEZ, J. & CAMPOS-PENA, V. 2013. Inflammatory process in Alzheimer's Disease. *Front Integr Neurosci*, 7, 59.
- MORRIS, J. C., ROE, C. M., XIONG, C., FAGAN, A. M., GOATE, A. M., HOLTZMAN, D. M. & MINTUN, M. A. 2010. APOE predicts amyloid-beta but not tau Alzheimer pathology in cognitively normal aging. *Ann Neurol*, 67, 122-31.
- NAKAJIMA, T., AMANUMA, R., UEKI-MARUYAMA, K., ODA, T., HONDA, T., ITO, H. & YAMAZAKI, K. 2008. CXCL13 expression and follicular dendritic cells in relation to B-cell infiltration in periodontal disease tissues. *J Periodontal Res*, 43, 635-41.
- PARK, M. H., LEE, J. K., CHOI, S., AHN, J., JIN, H. K., PARK, J. S. & BAE, J. S. 2013. Recombinant soluble neprilysin reduces amyloid-beta accumulation and improves memory impairment in Alzheimer's disease mice. *Brain Res*, 1529, 113-24.
- PRASAD, R. Y., MCGEE, J. K., KILLIUS, M. G., SUAREZ, D. A., BLACKMAN, C. F., DEMARINI, D. M. & SIMMONS, S. O. 2013. Investigating oxidative stress and inflammatory responses elicited by silver nanoparticles using high-throughput reporter genes in HepG2 cells: effect of size, surface coating, and intracellular uptake. *Toxicol In Vitro*, 27, 2013-21.

- QUADROS, M. E. & MARR, L. C. 2010. Environmental and human health risks of aerosolized silver nanoparticles. *J Air Waste Manag Assoc*, 60, 770-81.
- RAHMAN, M. F., WANG, J., PATTERSON, T. A., SAINI, U. T., ROBINSON, B. L., NEWPORT, G. D., MURDOCK, R. C., SCHLAGER, J. J., HUSSAIN, S. M. & ALI, S. F. 2009. Expression of genes related to oxidative stress in the mouse brain after exposure to silver-25 nanoparticles. *Toxicol Lett*, 187, 15-21.
- RIBEIRO, F., GALLEGU-URREA, J. A., JURKSCHAT, K., CROSSLEY, A., HASSELLOV, M., TAYLOR, C., SOARES, A. M. & LOUREIRO, S. 2013. Silver nanoparticles and silver nitrate induce high toxicity to *Pseudokirchneriella subcapitata*, *Daphnia magna* and *Danio rerio*. *Sci Total Environ*, 466-467C, 232-241.
- SELENICA, M. L., ALVAREZ, J. A., NASH, K. R., LEE, D. C., CAO, C., LIN, X., REID, P., MOUTON, P. R., MORGAN, D. & GORDON, M. N. 2013. Diverse activation of microglia by chemokine (C-C motif) ligand 2 overexpression in brain. *J Neuroinflammation*, 10, 86.
- SHARMA, H. S. & SHARMA, A. 2012. Neurotoxicity of engineered nanoparticles from metals. *CNS Neurol Disord Drug Targets*, 11, 65-80.
- SINGH, R. P. & RAMARAO, P. 2012. Cellular uptake, intracellular trafficking and cytotoxicity of silver nanoparticles. *Toxicol Lett*, 213, 249-59.
- SMITH, M. P. & CASS, W. A. 2007. Oxidative stress and dopamine depletion in an intrastriatal 6-hydroxydopamine model of Parkinson's disease. *Neuroscience*, 144, 1057-66.
- SOFRONIEW, M. V. & VINTERS, H. V. 2010. Astrocytes: biology and pathology. *Acta Neuropathol*, 119, 7-35.
- TANG, J., XIONG, L., WANG, S., WANG, J., LIU, L., LI, J., YUAN, F. & XI, T. 2009. Distribution, translocation and accumulation of silver nanoparticles in rats. *J Nanosci Nanotechnol*, 9, 4924-32.
- TANG, J., XIONG, L., ZHOU, G., WANG, S., WANG, J., LIU, L., LI, J., YUAN, F., LU, S., WAN, Z., CHOU, L. & XI, T. 2010. Silver nanoparticles crossing through and distribution in the blood-brain barrier in vitro. *J Nanosci Nanotechnol*, 10, 6313-7.
- TAPPIN, A. D., BARRIADA, J. L., BRAUNGARDT, C. B., EVANS, E. H., PATEY, M. D. & ACHTERBERG, E. P. 2010. Dissolved silver in European estuarine and coastal waters. *Water Res*, 44, 4204-16.
- VERANO-BRAGA, T., MIETHLING-GRAFF, R., WOJDYLA, K., ROGOWSKA-WRZESINSKA, A., BREWER, J. R., ERDMANN, H. & KJELDTSEN, F. 2014. Insights into the cellular response triggered by silver nanoparticles using quantitative proteomics. *ACS Nano*, 8, 2161-75.
- WANG, S., WANG, R., CHEN, L., BENNETT, D. A., DICKSON, D. W. & WANG, D. S. 2010. Expression and functional profiling of neprilysin, insulin-degrading enzyme, and endothelin-converting enzyme in prospectively studied elderly and Alzheimer's brain. *J Neurochem*, 115, 47-57.
- WANG, Y., WANG, B., ZHU, M. T., LI, M., WANG, H. J., WANG, M., OUYANG, H., CHAI, Z. F., FENG, W. Y. & ZHAO, Y. L. 2011. Microglial activation, recruitment and phagocytosis as linked phenomena in ferric oxide nanoparticle exposure. *Toxicol Lett*, 205, 26-37.

- WEI, J., GABRUSIEWICZ, K. & HEIMBERGER, A. 2013. The controversial role of microglia in malignant gliomas. *Clin Dev Immunol*, 2013, 285246.
- WEISS, N., MILLER, F., CAZAUBON, S. & COURAUD, P. O. 2009. The blood-brain barrier in brain homeostasis and neurological diseases. *Biochim Biophys Acta*, 1788, 842-57.
- WIJNHOFEN, S. W. P., PEIJNENBURG, W. J. G. M., HERBERTS, C. A., HAGENS, W. I., OOMEN, A. G., HEUGENS, E. H. W., ROSZEK, B., BISSCHOPS, J., GOSENS, I., VAN DE MEENT, D., DEKKERS, S., DE JONG, W. H., VAN ZIJVERDEN, M., SIPS, A. J. A. M. & GEERTSMA, R. E. 2009. Nano-silver - a review of available data and knowledge gaps in human and environmental risk assessment. *Nanotoxicology*, 3, 109-U78.
- XU, F., PIETT, C., FARKAS, S., QAZZAZ, M. & SYED, N. I. 2013. Silver nanoparticles (AgNPs) cause degeneration of cytoskeleton and disrupt synaptic machinery of cultured cortical neurons. *Mol Brain*, 6, 29.
- XU, P. X., WANG, S. W., YU, X. L., SU, Y. J., WANG, T., ZHOU, W. W., ZHANG, H., WANG, Y. J. & LIU, R. T. 2014. Rutin improves spatial memory in Alzheimer's disease transgenic mice by reducing A β oligomer level and attenuating oxidative stress and neuroinflammation. *Behav Brain Res*, 264, 173-80.

**Silver nanoparticles affect on gene expression of inflammatory and
neurodegenerative responses in mouse brain neural cells**

**Chin-Lin Huang, I-Lun Hsiao, Ho-Chen Lin, Chu-Fang Wang, Yuh-Jeen Huang*,
Chun-Yu Chuang***

*Department of Biomedical Engineering and Environmental Sciences, National Tsing
Hua University, Hsinchu, Taiwan*

*Corresponding Author:

Chun-Yu Chuang

Department of Biomedical Engineering and Environmental Sciences

National Tsing Hua University

101, section 2, Kuang-Fu Road, Hsinchu 30013, Taiwan.

E-mail: cychuang@mx.nthu.edu.tw

Phone: +886-3-5715131 ext 34229

Fax: +886-3-5718649

Yuh-Jeen Huang

Department of Biomedical Engineering and Environmental Sciences

National Tsing Hua University

101, section 2, Kuang-Fu Road, Hsinchu 30013, Taiwan.

email: yjhuang@mx.nthu.edu.tw

Phone: +886-3-5715131 ext 35496

Fax: +886-3-5718649

E-mail: yjhuang@mx.nthu.edu.tw

Abstract

1 Silver nanoparticles (AgNPs) have antibacterial characteristics, and currently are
2
3
4 applied in Ag-containing products. This study found neural cells can uptake 3-5 nm
5
6
7 AgNPs, and investigated the potential effects of AgNPs on gene expression of
8
9
10 inflammation and neurodegenerative disorder in murine brain ALT astrocytes,
11
12
13 microglial BV-2 cells and neuron N2a cells. After AgNPs (5, 10, 12.5 $\mu\text{g/ml}$) exposure,
14
15
16 these neural cells had obviously increased IL-1 β secretion, and induced gene
17
18
19 expression of C-X-C motif chemokine 13 (*CXCL13*), macrophage receptor with
20
21
22 collagenous structure (*MARCO*) and glutathione synthetase (*GSS*) for inflammatory
23
24
25 response and oxidative stress neutralization. Additionally, this study found amyloid- β
26
27
28 ($\text{A}\beta$) plaques for pathological feature of Alzheimer's disease (AD) deposited in neural
29
30
31 cells after AgNPs treatment. After AgNPs exposure, the gene expression of amyloid
32
33
34 precursor protein (*APP*) was induced, and otherwise, neprilysin (*NEP*) and low-density
35
36
37 lipoprotein receptor (*LDLR*) were reduced in neural cells as well as protein level. These
38
39
40 results suggested AgNPs could alter gene and protein expressions of $\text{A}\beta$ deposition
41
42
43 potentially to induce AD progress in neural cells. It's necessary to take notice of
44
45
46 AgNPs distribution in the environment.
47
48
49
50
51
52
53
54

55 Keywords: silver nanoparticle; inflammation; gene expression; neurodegenerative
56
57
58 disorder; Alzheimer's disease
59
60
61
62
63
64
65

1. Introduction

1 In recent years, nanotechnology grows rapidly, and nanoparticles are produced and
2
3
4 widely utilized in diverse areas of different industrial applications because of its high
5
6
7 interfacial reactivity and unique physicochemical properties (Loo et al., 2013). As to
8
9
10 antibacterial / antifungal characteristics, silver nanoparticles (AgNPs) have been used
11
12
13 in clothes, cosmetics, wound dressing, air-freshener sprays, water disinfectant,
14
15
16 sunscreens, hygiene products and food containers, which increases the release of
17
18
19 nanoparticles to environment and may cause exposure to human (Ribeiro et al., 2013).
20
21
22 The exposure route for AgNPs happens via ingestion, inhalation or dermal contact.
23
24
25
26 Kulthong et al. (2010) indicated that the antibacterial fabric from six commercial
27
28
29 fabrics releases silver of AgNPs when is immersed in artificial sweat as a model to
30
31
32 represent the human skin environment. In addition, AgNPs may have an access to
33
34
35 systemic circulation through broken skin when we use the AgNP-containing products
36
37
38 such as bandages or wound dressings (Singh and Ramarao, 2012). After injection
39
40
41 different particles size of Ag (nanosized and microsized) in rats (62.8 mg/kg), AgNPs
42
43
44 can translocate to the blood circulation and distribute throughout the main organs,
45
46
47 especially in the kidney, liver, spleen, lung and brain, and induce blood-brain barrier
48
49
50 (BBB) destruction and astrocyte swelling to cause neuronal degeneration (Tang et al.,
51
52
53 2009).
54
55
56

57
58 Ag is one of the most toxic metals for the marine systems (Tappin et al., 2010), and
59
60
61 the monovalent silver ion is considered as the most toxic silver species in aquatic
62
63
64 systems and causes intracellular accumulation in phytoplankton (Lee et al., 2005).
65

1
2
3
4
5
6
7
8
9
10
11
12
13
14
15
16
17
18
19
20
21
22
23
24
25
26
27
28
29
30
31
32
33
34
35
36
37
38
39
40
41
42
43
44
45
46
47
48
49
50
51
52
53
54
55
56
57

However, the AgNPs (<100 nm, 0.5 and 1 ug/ml) cause nuclear condensation and induce higher dramatically cytotoxicity than Ag ions in human lymphoma cells (Eom and Choi, 2010). In addition, a proteomic analysis showed that 20 nm AgNPs interfere with protein regulations of mitochondrial translation, RNA processing, tRNA metabolism and cell proliferation more than Ag ions and larger size AgNPs (100 nm) in human colon adenocarcinoma LoVo cells (Verano-Braga et al., 2014). The diameter 139±37 nm AgNPs trigger dose-dependent effect of decreased cell viability on human lung carcinoma A549 cells in exposure to 5, 10 and 15 ug/ml AgNPs (Foldbjerg et al., 2011). Besides, the cell deaths in apoptosis and necrosis all increase after exposure to AgNPs (2.5, 5, 10 and 15 µg/ml). Moreover, Gaiser et al. (2013) pointed that 20 nm diameter nanoparticles can cause toxicity, inflammation and oxidative stress after exposure to human C3A hepatocytes and female Wistar rats. Besides, the inflammatory cytokines, e.g., IL-8, MIP2, IL-1RI and TNF-α, are both increased on *in vitro* and *in vivo* models after AgNPs-induction. Overall, the Ag and Cu nanoparticles can easily enter the mice brain to disrupt BBB permeability and induce neurotoxicity, which alters brain sensory, motor and cognitive functions (Sharma and Sharma, 2012). AgNPs (20 nm; 1, 5, 10 and 50 µg/ml) can reduce cell viability in primary rat cortical cells, and inhibit the sprouting of neuronal branches and elongation of neuritis for fragmentation and degeneration of mature neurons (Xu et al., 2013).

58
59
60
61
62
63
64
65

Brain is composed of endothelial cells, neurons and glial cells. Astrocytes are known as reactive astrogliosis cells to regulate metal homeostasis, supply nutrients to neurons and protect other brain cells against oxidative stress and metal toxicity (Sofroniew and

Vinters, 2010). Microglia are a type of glial cell major brain-resident macrophage-like cells in the central nerve system (CNS) to defend against microorganism invasion and injury, and release some cytokine factors to mediate neuroinflammatory processes (Wang et al., 2011). The inflammatory response, a tissue reaction to injury or an antigen, releases cytokines, chemokines, reactive oxygen species (ROS) and nitric oxides (NO) (Wei et al., 2013). Nerve cells connect to each other to form neural networks. Neurons are electrically excitable brain endothelium to transmit information through electrical and chemical signals via synapses and contact with perivascular astrocytes and pericytes (Weiss et al., 2009). Tang et al. (2010) indicated that AgNPs can cross through the BBB of rat brain to influence brain cells through transcytosis of capillary endothelial cells detectable by transmission electronic microscopy (TEM) and inductively-coupled plasma mass spectrometry (ICP-MS). Thus, the highest concentration of silver is observed in the kidneys and brain 28 days after injection a dose 5 mg kg⁻¹ bw AgNPs (20 and 200 nm) in Wistar rats (Dziendzikowska et al., 2012). Haase et al. (2012) found that AgNPs increase ROS generation and heme oxygenase 1 (HO-1) protein expression to cause neuronal oxidative damage and directly interfere with calcium responses in primary mixed neural cells. Increased levels of ROS occurred chronically in the early disease, which is relevant to neurodegenerative disorders, such as Alzheimer's and Parkinson's disease (Smith and Cass, 2007). Moreover, glutathione metabolism plays an important role of protecting cell from oxidative stress, and their gene expression related to oxidative stress are significantly altered in the caudate, frontal cortex and hippocampus of male C57BL/6N

mice after administered 25 nm AgNPs (Rahman et al., 2009).

1 The C-X-C motif chemokine 13 (*CXCL13*) play a role in the B-cell recruitment and
2
3
4 distribution, associated with chronic inflammatory process (Nakajima et al., 2008).
5
6
7 Macrophage receptor with collagenous structure (*MARCO*) is important for immune
8
9
10 responses to bacterial infections by mediating the binding and phagocytosis of
11
12
13 pathogens (Komine et al., 2013). Accordingly, studies have indicated that AgNPs can
14
15
16 induce ROS and cytokines increasing and then cause inflammatory response. As
17
18
19 *CXCL13* and *MARCO* genes are immune mediators in response to inflammation,
20
21
22 exposure to AgNPs may change their gene expression. Moreover, glutathione
23
24
25 synthetase (*GSS*) can synthesize glutathione (*GSH*) potentially to inhibit oxidative
26
27
28 stress and prevent cellular damage from free radicals and peroxides (Koike et al., 2013),
29
30
31 and AgNPs exposure probably alters *GSS* gene expression.
32
33
34

35 Amyloid beta ($A\beta$) is a peptide of amino acids that is processed from amyloid
36
37
38 precursor protein (*APP*). $A\beta$ protein is considered the main responsible for
39
40
41 neurodegenerative disorder such as Alzheimer's disease (*AD*). The up-regulation of
42
43
44 *APP* gene expression interferes with $A\beta$ metabolism underlying the pathogenesis of
45
46
47 *AD* (Dong et al., 2012). Low-density lipoprotein receptor (*LDLR*) enhances $A\beta$ uptake
48
49
50 and degradation through binding $A\beta$ and $A\beta$ / ApoE complex (Basak et al., 2012). Thus,
51
52
53 the down-regulation of *LDLR* gene leads $A\beta$ deposition. Besides, neprilysin (*NEP*) is a
54
55
56 major $A\beta$ -degrading enzyme in brain to degrade $A\beta$ protein (El-Amouri et al., 2007).
57
58
59 Sequentially, it is important to investigate the receptors and gene expression regulating
60
61
62 $A\beta$ amyloid internalization in neural cells for understanding the *AD* pathogenesis.
63
64
65

1 According to previous studies, the information until now is not well known that
2 whether the AgNPs-induced neuroinflammation cause the changes in gene expression
3 related neurodegenerative disorder such as AD. In this study, we investigated whether
4 the 3-5 nm AgNPs can pass through mouse brain neuronal cells and induce A β amyloid
5 generation underlying the potential effect of AgNPs on gene expression of
6 inflammatory response, oxidative stress, and A β deposition.
7
8
9
10
11
12
13
14
15
16
17
18
19

20 **2. Material and methods**

21 2.1 Cell culture and exposure

22
23 This study used three types of neural cells, murine brain ALT astrocytes (BCRC
24 60581), murine microglial BV-2 cells (ICLC ATL03001) and mouse neuroblastoma
25 Neuro-2a (N2a) cells (BCRC 60026). N2a cells were cultured in high glucose
26 Dulbecco's Modified Eagle's Medium (DMEM; CORNING, New York) supplemented
27 with 10 percent fetal bovine serum (Invitrogen, Carlsbad, Canada), 1 percent antibiotic
28 (Biowest, Loire Valley, France), 1 percent L-glutamine (Invitrogen), 1 percent sodium
29 pyruvate (Invitrogen) in a cell incubator with 5 percent CO₂ at 37 °C. ALT cells and
30 BV-2 cells were cultured in the similar medium with N2a cells except for the lack of 1
31 percent sodium pyruvate. When N2a cells grew to 70-80 percent confluence of a
32 culture plate, the growth medium was removed and replaced with differentiation
33 medium for two days. The Differentiation medium containing forskolin and
34 isobutylmethylxanthine (IBMX) was added to N2a cells for 24 h differentiation. N2a
35 cells can be differentiated into a neuron-like morphology with expression of several
36
37
38
39
40
41
42
43
44
45
46
47
48
49
50
51
52
53
54
55
56
57
58
59
60
61
62
63
64
65

1 neuronal markers. The 3-5 nm AgNPs were produced by a physical method without
2 surfactants or stabilizers (Gold Nanotech Inc., Taiwan). AgNPs (0.5, 1, 5, 10 and 12.5
3 $\mu\text{g/ml}$) and lipopolysaccharides (LPS; 0.2 and 2 $\mu\text{g/ml}$; Invitrogen) were respectively
4 added into the medium to treat ALT, BV-2 and N2a cells for 24 h exposure.
5
6
7
8
9

10 11 12 13 2.2 Polarizing microscope 14 15

16 N2a cells were cultured on glass coverslips with the treatment of AgNPs (5 nm, 12.5
17 $\mu\text{g/ml}$) for 24 h. After treatment, the cells on coverslips were fixed in 4 percent
18 paraformaldehyde (PFA) for 10 min at 4°C, then washed with phosphate buffered
19 saline (PBS) and mounted with slides in mountain medium. Images of AgNPs location
20 were captured under the polarizing microscopy (IX71, Olympus, Tokyo, Japan).
21
22
23
24
25
26
27
28
29
30
31

32 33 34 35 2.3 Cell proliferation of neural cells 36 37

38 The neural cells $1 \times 10^4 \text{ cm}^{-2}$ were seeded in 96-well plates for cell viability analysis.
39 After exposure to AgNPs or LPS, the suspensions were discarded, alamarBlue®
40 reagent (DMEM / 10 percent FBS 1:10; Invitrogen) was added as a cell viability
41 indicator followed by a 2 h incubation at 37°C, and the absorbance was monitored at
42 570 nm using 600 nm as a reference wavelength. The cell viability was calculated as
43
44
45
46
47
48
49
50
51
52
53
54
55
56
57
58
59
60
61
62
63
64
65

[cell number of exposure samples] / [cell number of control] \times 100. Cell numbers were derived from a standard curve, which was obtained after seeding serially diluted cells (from 5×10^4 to 1.56×10^3 cells/ml) in a 96-well plate.

2.4 Cytokine assay of IL-1 β

1 The concentrations of pro-inflammatory cytokine IL-1 β were determined using
2
3
4 ELISA kits (Mouse IL-1 β Instant ELISA, eBioscience, San Diego, Canada) according to
5
6
7 the operation manual. A 96-well plate was coated with capture antibody (purified
8
9
10 anti-mouse IL-1 β) in coating buffer and incubated overnight at 4°C. After three time
11
12
13 wash with PBST (PBS with 1 percent Tween 20), the blocking solution (200 μ l) was
14
15
16 added to each well with 1 h. After wash, the samples (100 μ l) and IL-1 β standards
17
18
19 (16-2000 pg/ml) were added to each well for 2 h incubation at room temperature. After
20
21
22 incubation and wash, the 100 μ l of biotin-conjugated anti-mouse IL-1 β and
23
24
25 streptavidin-horseradish peroxidase (HRP) were added to each well for 30 min
26
27
28 incubation, then wash, and each well was added to 100 μ l TMB
29
30
31 (3,3',5,5'-Tetramethylbenzidine) substrate solution for 15 min. Final, the 50 μ l stop
32
33
34 solution (2 M H₂SO₄) was added to each well and the optical density was determined at
35
36
37 450 nm using a VERSAmax microplate reader (Molecular Devices, Sunnyvale,
38
39
40
41
42 Canada).

2.5 Immunofluorescent detection of A β protein

51 N2a cells cultured on coverslips were washed twice with 1X PBS and then fixed
52
53
54 with 4 percent PFA for 10 min at 4°C, and washed with PBS. Cells were permeabilized
55
56
57 with 0.1 percent Triton X-100 / PBS solution at room temperature for 30 min, blocked
58
59
60 in 2 percent horse serum (HS) at room temperature for 30 min, and then incubated for
61
62
63 1 h respectively with primary rabbit anti-mouse A β ₁₋₄₀ (1:500; Cat. 171608, Merck
64
65

1
2
3
4
5
6
7
8
9
10
11
12
13
14
15
16
17
18
19
20
21
22
23
24
25
26
27
28
29
30
31
32
33
34
35
36
37
38
39
40
41
42
43
44
45
46
47
48
49
50
51
52
53
54
55
56
57
58
59
60
61
62
63
64
65

Millipore, Darmstadt, Germany) or primary rabbit anti-mouse A β ₁₋₄₂ (1:500; Cat. 171609, Merck Millipore). The coverslips were then washed three times with PBS and stained with secondary fluorescein isothiocyanate (FITC)-conjugated goat anti-rabbit IgG (1:500; Cat. 12-507, Merck Millipore). After washed in PBS, the coverslips were incubated with Hoechst 33258 (1:20; Cat. 23491-45-4, Sigma-Aldrich, St. Louis, MO) and rinsed in PBS. Coverslips were mounted on slides in mountain medium. Immunofluorescence images were captured with an inverted microscope with fluorescence filters (Axio Observer A1/D1, Zeiss, Oberkochen, Germany).

2.6 RNA extraction

Total RNA was isolated respectively from ALT, BV-2 and N2a cells in exposure to AgNPs after 24 h using RNA Trizol (Invitrogen). After the culture medium were removed, neural cells were dissolved in 1 ml of TRIZOL reagent, and then 0.2 ml chloroform was added a 1.5 ml eppendorf tube. The mixture was shook vigorously for 15 s and centrifuged at 12,000 g for 15 min at 4°C. Next, the supernatant was transferred to a fresh tube, and 0.5 ml isopropanol (SIGMA) was added at room temperature for 10 min. The RNA was precipitated after centrifugation at 12,000 g for 10 min at 4°C. The RNA pellet was washed with 1 ml of 75 percent ethanol (Taiwan Tobacco & Liquor Corporation, Taipei, Taiwan) and centrifuged at 7500 g for 5 min at 4°C to remove the ethanol. The RNA pellet was dried up and diluted with RNase-free water. The purified RNA was quantified using Nanodrop 2000c (Thermo, Wilmington, Massachusetts).

2.7 Reverse transcription polymerase chain reaction (RT-PCR)

cDNA was synthesized from total RNA by a high-capacity cDNA reverse transcription kit (Applied Biosystems, California). The 3 µg RNA was added 1.0 µl MultiScribe™ reverse transcriptase (50 unit µl⁻¹), 2.0 µl 10X RT random primers, 0.8 µl 20X concentrated dNTP mix, 2.0 µl 10X concentrated RT buffer and RNase free water (DEPC water) in a 0.2 ml PCR tube, and subsequently amplified by PCR with one cycle of 20°C 10 min, 37°C 120 min and 85°C 5 s.

2.8 Real time PCR for gene expression quantitation

One hundred nanograms cDNA was a was amplified by PCR with 40 cycles of denaturing (95°C, 15 s), annealing (55°C, 30 s) and extension (72°C, 45 s) using 2X power SYBR green PCR master mix (Applied Biosystems). PCR primers: *CXCL13* sense 5'-ATG TGT GAA TCC TCG TGC CAA-3' and anti-sense 5'-AAA AAA GGT GCA GGT GTG TCT-3'; *MARCO* sense 5'-GGG TCA AAA AGG CGA ATC T-3' and anti-sense 5'-ATG TTC CCA GAG CCA CCT-3'; *GSS* sense 5'-GGT ATC TTC CCT CAG CAG CCT T-3' and anti-sense 5'-GCT TCC ATT CCC ACA CTC CAA A-3'; *APP* sense 5'-CTG GAC GGT TCG GGC TCT-3' and anti-sense 5'-CGG GTC TGA CTC CCA CTT TC-3'; *LDLR* sense 5'-TCC AAT CAA TTC AGC TGT GGA G-3' and anti-sense 5'-ATC AGA GCC ATC TAG GCA ATC TCG-3'; *NEP* sense 5'-AAA GCC AAA GAA GAA ACA GCG A-3' and anti-sense 5'-GCA TAG AGA GCG ATC ATT GTC ACC G-3'; *β-actin* sense 5'-ATG CTC CCC GGG CTG TAT-3'

and anti-sense 5'-CCA CTG CTC CGG GTC TCG-3'. Quantitative analysis of PCR products was carried out by a sequence detector (Model 7300, Applied Biosystems) according to the manufacturer's instruction. The signal of SYBR green was measured at 530 nm during extension phase, and collected and analyzed with SDS 1.0 software. The threshold cycle (Ct) value denotes the cycle number at which the fluorescence generated within a reaction across the threshold, thus the Ct value is at the point accumulated a sufficient number of amplicons during the reaction. The relative level of mRNA expression is a ratio of optical density of the experimental groups to that of *β-actin* (internal control, an endogenous house-keeping gene). The relative Ct value of different condition was compared to that of control cells as reference to estimate the fold change of mRNA expression among the samples. Triplicates were performed for each primer pair.

2.9 Western blotting for protein determination

N2a cells were lysed with RIPA buffer (Cell Signaling, Danvers, MA) containing proteinase inhibitor Cocktail (Sigma), and centrifuged at 8,000 g for 3 min at 4°C. Protein samples in the supernatant were immediately transferred, and the concentration was measured using a Bicinchoninic Acid Protein Assay Kit (Sigma). Protein in the samples were then electrophoresed over a 10% sodium dodecyl sulfate polyacrylamide gel, and subsequently transferred to a hydrophobic PVDF membrane (Millipore). The membrane-bound proteins were respectively immunostained with 1:1000 primary rabbit anti-mouse NEP (CD10) (Cat. EPR 2997, Abcam, Cambridge, MA), APP (Cat.

1 Biotechnology, Senta Cruz, CA) antibody and followed by treatment with secondary
2
3
4 anti-rabbit IgG horse radish peroxidase (HRP) antibody (Senta Cruz Biotechnology,
5
6
7 CA). The tagged proteins were detected using a chemiluminescence reagent
8
9
10 (Thermo Scientific, Rockford, IL) and photographed in a G:Box ChemiXT 16 system
11
12
13 (Syngene, Frederick, MD). The band intensities in the western blots were quantified by
14
15
16 ImageJ software.
17
18
19
20
21
22

23 2.10 Statistical analysis 24 25

26 Results were described as mean \pm standard deviation. Data analysis was conducted
27
28
29 by the statistical package SPSS 13.0 (SPSS Inc., Chicago, Illinois). The statistically
30
31
32 significant differences of cell proliferation, IL-1 β , gene expression and protein
33
34
35 respectively between AgNPs treatment and control were analyzed using Student's *t* test.
36
37
38

39 All statistical significances were determined at two-tailed *p* value < 0.05.
40
41
42
43
44
45
46
47
48
49
50
51
52
53
54
55
56
57
58
59
60
61
62
63
64
65

3. Results

3.1 Permeability, cytotoxicity and pro-inflammation of AgNPs in neural cells

The zeta potential of the 3-5 nm AgNPs used in this study was -4.2 mV in culture medium. The 3-5 nm AgNPs (12.5 $\mu\text{g/ml}$) can cross the cell membrane of N2a cells detectable under polarizing microscope (Fig. 1). The cell proliferation of ALT, BV-2 and N2a cells exposed to AgNPs (0.5, 1, 5, 10 and 12.5 $\mu\text{g/ml}$) and LPS (0.2, 2 $\mu\text{g/ml}$) for 24 h were shown in Fig. 2. The cell proliferation was decreased in ALT cells (0.5, 1, 10 and 12.5 $\mu\text{g/ml}$) and N2a cells (12.5 $\mu\text{g/ml}$) but not differently changed in BV-2 cells after AgNPs exposure. LPS decreased cell proliferation obviously in ALT cells (2 $\mu\text{g/ml}$) and BV-2 cells (0.2 $\mu\text{g/ml}$). Additionally, the IL-1 β secretion of ALT, BV-2 and N2a cells was detected after 24 h AgNPs exposure (Fig. 3). IL-1 β protein was significantly increased in BV-2 cells after 12.5 $\mu\text{g/ml}$ AgNPs exposure.

3.2 A β amyloid deposition in neural cells after AgNPs exposure

The immunofluorescence images revealed that A β_{1-40} (Fig. 4) and A β_{1-42} (Fig. 5) proteins were inducible to generate after AgNPs exposure 12.5 $\mu\text{g/ml}$ in N2a cells, and detectable in a fluorescence microscope.

3.3 Gene expression of neural cells in exposure to AgNPs

LPS induced the expression of *CXCL13* and *MARCO* genes for inflammatory process and phagocytosis. The gene expression of *CXCL13* and *MARCO* were increased in ALT, BV-2 and N2a cells at the higher dose of AgNPs (5, 10 and 12.5

1 $\mu\text{g/ml}$) (Fig. 6A and 6B). The *GSS* mRNA level was significantly decreased in ALT
2 cells (0.5, 1, 5, 10 and 12.5 $\mu\text{g/ml}$) and increased in BV-2 cells (10 and 12.5 $\mu\text{g/ml}$)
3
4 after AgNPs exposure (Fig. 6C). On the other hand, the gene expression of AD process
5
6 related genes such as *APP*, *LDLR* and *NEP* were also altered in exposure to AgNPs.
7
8 The gene expression of *APP* was elevated in ALT, BV-2 (5, 10 and 12.5 $\mu\text{g/ml}$) and
9
10 N2a (12.5 $\mu\text{g/ml}$) cells (Fig. 6D). On the contrary, the decreased *LDLR* mRNA level
11
12 was observed in 12.5 $\mu\text{g/ml}$ AgNPs-treated ALT, BV-2 and N2a cells (Fig. 6E). *NEP*
13
14 gene expression also reduced significantly in N2a cells exposed to AgNPs (Fig. 6F).
15
16
17
18
19
20
21
22
23
24
25

26 3.4 Protein determination of neural cells in exposure to AgNPs

27
28
29 The protein levels of APP, LDLR and NEP were determined after N2a cells exposed
30
31 to 1, 5, 10, 12.5 and 15 $\mu\text{g/ml}$ AgNPs, respectively. APP levels were obviously induced
32
33 in exposure to 10, 12.5 and 15 $\mu\text{g/ml}$ AgNPs (Fig. 7A). LDLR levels were significantly
34
35 reduced after exposure to 1, 10 and 15 $\mu\text{g/ml}$ AgNPs (Fig. 7B). The level of NEP
36
37 protein was increased after AgNPs and returned to the steady state as control group
38
39 (Fig. 7C).
40
41
42
43
44
45
46
47
48
49

50 4. Discussion

51
52
53 This study found that 3-5 nm AgNPs can cross the cell membrane (Fig. 1), induced
54
55 IL-1 β secretion for inflammatory response (Fig. 3), and accelerate A β 1-40 (Fig. 4) and
56
57 A β 1-42 (Fig. 5) generation and deposition. AgNPs exposure (5, 10, 12.5 $\mu\text{g/ml}$)
58
59 induced the gene expression of *CXCL13*, *MARCO* and *GSS* for inflammatory response
60
61
62
63
64
65

and oxidative stress (Fig. 6). Besides, AgNPs exposure increased the gene expression and protein level of APP for A β generation, and reduced LDLR and NEP for A β uptake/transporter and A β degradation (Fig. 6 and Fig. 7). These findings suggested that AgNPs exposure potentially caused neurodegenerative disorder progression underlying A β deposition.

4.1 AgNPs exposure induced inflammatory response in mouse neural cells

This study found that AgNPs crossed the cell membrane of neuron cells and mostly distributed in the cytoplasm (Fig. 1), and induced IL-1 β secretion (Fig. 3) for inflammatory response in neural cells (astrocytes, microglia and neuron cells). AgNPs and iron oxide nanoparticles in astrocytes are internalized by endocytotic uptake processes into cellular vesicles to respectively release Ag and ferrous iron and induce ROS generation and inflammation (Hohnholt et al., 2013). Prasad et al. (2013) indicated that AgNPs have a higher rate of cellular uptake compared with AgNO₃ and cause oxidative stress and inflammatory response in liver HepG2 cells. Moreover, AgNPs can enter the brain through the olfactory nerve, and the toxic effect of AgNPs is stronger than silver ions because ions are consumed before reaching the cell membrane (Wijnhoven et al., 2009, Quadros and Marr, 2010). Besides, in the analysis of Mouse Oxidative Stress and Antioxidant Defense Arrays, male C57BL/6N mice administered with 25 nm AgNPs change the expression of oxidative stress associated genes in the caudate, frontal cortex and hippocampus (Rahman et al., 2009).

The results of this study indicated that AgNPs activated stress-responsive gene *GSS*

and immune reaction genes *CXCL13* and *MARCO*. AgNPs induces inflammatory cytokine TNF- α release, ROS and endoplasmatic reticulum (ER) stress response in zebrafish liver cells (Christen et al., 2013). Cha et al. (2008) found the AgNPs-treated liver cells have the up-regulated gene expression of *CXCL13* and *MARCO* to induce apoptosis and inflammation. Moreover, chemokine C-C motif ligand (CCL) 2 can activate resident microglias in the brain to recruit peripheral macrophages and increase chemokine family *CCL24* gene expression (Selenica et al., 2013). Kang et al. (2012) reported that 7.5 ± 2.5 nm AgNPs evoke ROS generation and increase a major cellular thiol antioxidant GSH level in human renal proximal tubular epithelial HK-2 cells. Importantly, the diameter of 20 and 40 nm AgNPs (10 and 20 $\mu\text{g/ml}$) can lead to mixed primary cortical neural cells increase the level of ROS in accompanied with calcium rises, and the smaller AgNPs have stronger cytotoxicity than bigger ones (Haase et al., 2012).

4.2 AgNPs exposure changed gene expression and protein level of amyloid plaque deposition in mouse neuron cells

Neuroinflammation and beta-amyloid deposition led to memory impairment in Alzheimer's disease transgenic mice (Xu et al., 2014). According to above studies, we inferred that chronic ROS increase and unbalance calcium level in neural cells may cause AD neurodegenerative disorder. This study observed that AgNPs caused A β amyloid plaque deposition in mouse neuron N2a cells (Fig. 4 and Fig. 5). Furthermore, this study determined the gene expression corresponding to A β generation and

deposition in neural cells treated with AgNPs (Fig. 6).

1 The ability of insoluble 40 to 42 peptides of A β amyloid has been considered more
2
3 rapidly aggregation and more neurotoxicity in AD progression (Landau et al., 2013). In
4
5 this study, AgNPs exposure can induce A β_{1-40} and A β_{1-42} peptides aggregation in neural
6
7 cells (Fig. 4 and Fig. 5). Additionally, the gene expression (Fig. 6) and protein level
8
9 (Fig. 7) of A β amyloid generation and deposition relevant to AD progression have been
10
11 explored after AgNPs exposure. AgNPs induced the expression of *APP*, and otherwise,
12
13 attenuated *NEP* and *LDLR* for the potential effect on A β deposition. APP protein is an
14
15 integral membrane glycoprotein expressing in the brain and central nervous system,
16
17 and A β amyloid is produced by sequential cleavage of APP by β -secretase and
18
19 γ -secretase (Dong et al., 2012). The increased APP and β -secretase levels lead to
20
21 increase A β amyloid formation and aggregation potentially for neurodegenerative
22
23 disease (Meraz-Rios et al., 2013). The results of this study suggested that AgNPs led to
24
25 up-regulate the gene expression of *APP*, and down-regulate A β uptake gene *LDLR* and
26
27 A β degradation gene *NEP*. LDLR can enhance A β uptake and degradation to regulate
28
29 A β levels in the mouse brain (Basak et al., 2012). Cao et al. (2006) indicated that A β
30
31 deposition accompanies with the increased ApoE expression in *LDLR*-deficient Tg2576
32
33 mice. *LDLR*-deficient Tg2576 mice have disorders in hypercholesterolemia,
34
35 age-dependent cerebral β -amyloidosis and spatial learning deficits after A β deposition.
36
37 Thus, LDLR plays an important role in amyloidosis and the development of
38
39 Alzheimer-type learning impairment. NEP is the major protease involved in A β
40
41 degradation. The decreased *NEP* mRNA level is observed in AD patients (Wang et al.,
42
43
44
45
46
47
48
49
50
51
52
53
54
55
56
57
58
59
60
61
62
63
64
65

2010). AD patients have the significantly lower *NEP* mRNA and protein levels in the brain with high A β plaque burdens (Park et al., 2013).

4.3 The potential mechanism of AD pathogenesis in mouse neural cells exposure to AgNPs

This study observed that AgNPs activated the gene expression of *GSS*, *CXCL13* and *MARCO* for stress-response and immune reaction, and induced *APP* and attenuated *NEP* and *LDLR* genes for the potential effect on A β deposition. Regarding to our findings in this study, a schematic diagram illustrated in Fig. 8 described that AgNPs exposure in brain neural cells results in gene expression changes underlying the possible progression of A β plaque deposition for AD pathological feature. Inflammation elicits A β deposition via the activated microglia cells (Cameron and Landreth, 2010). This present study found AgNPs can enter into N2a cells and induce inflammatory response and A β deposition. The gene expression of *CXCL13*, *MARCO* and *GSS* in ALT, BV-2 and N2a cells are enhanced to defense against AgNPs-induced inflammatory reaction and oxidative stress. The APP protein is assembled from amino acids using information encoded in *APP* gene, which can be cleaved by α -secretase, β -secrease and γ -secrease to produce different length of A β peptides such as A β ₁₋₄₀ or A β ₁₋₄₂. Both of receptor for advanced glycation end product (RAGE) and low density lipoprotein receptor-related protein 1 (LRP1) are A β receptors able to bind A β or ApoE / A β complexes. RAGE transports A β proteins from blood to brain; in contrast, LRP1 transfers A β proteins from brain to blood (Kanekiyo et al., 2012, Han et al., 2011).

1 LDLR plays the main regulator with ApoE in CNS trafficking and breaking the balance
2 of A β levels. The different isoforms of ApoE play different function, the neutral ApoE3
3 and protective ApoE2 can support A β transport or degradation, and the AD-risk factor
4 ApoE4 accelerates A β aggregation for amyloid plaque formation (Morris et al., 2010).
5
6
7
8
9
10 There are sequential pathways to balance the A β levels in the brain, e.g., A β clearance
11 through BBB via RAGE and LRP1, A β degradation via NEP protease and
12 insulin-degrading enzyme (IDE), and A β deposition internalized in neural cells via
13 ApoE receptor when ApoE3 > ApoE4. AgNPs can activate *APP* gene to generate A β
14 amyloid, and disturb ApoE transport and reduce *NEP* and *LDLR* expression to
15
16
17
18
19
20
21
22
23
24
25
26
27
28
29
30
31
32
33
34
35
36
37
38
39
40
41
42
43
44
45
46
47
48
49
50
51
52
53
54
55
56
57
58
59
60
61
62
63
64
65

5. Conclusion

In summary, this study identified 3-5 nm AgNPs can enter in mouse neural cells to induce pro-inflammatory cytokine secretion and increase A β amyloid deposition in response to the changes of gene expression in inflammatory response, oxidative stress and A β degradation. These results suggested that AgNPs-induced neuroinflammatory response and A β deposition might evolve the progress of neurodegenerative disorders.

It is necessary to note the daily usage of silver nanoparticles.

Acknowledgement

We thank Gold Nanotech, Inc., Taiwan for providing AgNP materials in this collaborative research.

1
2
3
4
5
6
7
8
9
10
11
12
13
14
15
16
17
18
19
20
21
22
23
24
25
26
27
28
29
30
31
32
33
34
35
36
37
38
39
40
41
42
43
44
45
46
47
48
49
50
51
52
53
54
55
56
57
58
59
60
61
62
63
64
65

Figure Legends

1
2
3
4
5
6
7
8
9
10
11
12
13
14
15
16
17
18
19
20
21
22
23
24
Fig. 1 AgNPs uptake in mouse neuron N2a cells. A polarizing microscope was used to detect 5 nm AgNPs distribution in N2a cells. N2a cells were (A, B) cultured in normal culture medium, or (C, D) exposed to 12.5 $\mu\text{g/ml}$ AgNPs for 24 h. The bright field (A, C) and the dark field (B, D) indicate phase contrast image and polarizing image of corresponding cells respectively undertaken in 200X magnification with 30 μs and 10 ms exposure time. The red arrows point the location of AgNPs reflecting the bright spots mainly located inside the neural cells.

25
26
27
28
29
30
31
32
33
34
35
36
Fig. 2 Cell proliferation after exposure to AgNPs and LPS. Neural cells were treated with different concentration of 3-5 nm AgNPs (0.5, 1, 5, 10 and 12.5 $\mu\text{g/ml}$) and LPS (ALT 2 $\mu\text{g/ml}$, BV-2 0.2 $\mu\text{g/ml}$ and N2a 2 $\mu\text{g/ml}$) for 24 h. The data were presented as mean \pm SD (n=3). *indicates significant difference at $p < 0.05$ compared with control.

37
38
39
40
41
42
43
44
45
46
47
48
49
50
51
52
53
54
55
56
57
58
59
60
61
62
63
64
65
ALT: astrocyte, BV-2: microglia, N2a: neuron cells.

66
67
68
69
70
71
72
73
74
75
76
77
78
79
80
81
82
83
84
85
86
87
88
89
90
91
92
93
94
95
96
97
98
99
100
Fig. 3 Cytokines IL-1 β in neural cells after exposure to AgNPs and LPS. (A) ALT, (B) BV-2 and (C) N2a cells were respectively treated with different concentration of 3-5 nm AgNPs (5 and 12.5 $\mu\text{g/ml}$) and LPS (ALT 2 $\mu\text{g/ml}$, BV-2 0.2 $\mu\text{g/ml}$ and N2a 2 $\mu\text{g/ml}$) for 24 h. The data were presented as mean \pm SD (n=3). *indicates significant difference at $p < 0.05$ compared with control. ALT: astrocyte, BV-2: microglia, N2a: neuron cells.

Fig. 4 Amyloid- β_{1-40} plaques inside mouse neuron N2a cells in exposure to AgNPs.

1 Immunofluorescent detection of primary rabbit anti-mouse $A\beta_{1-40}$ was stained with
2
3
4 secondary goat FITC-conjugated anti-rabbit IgG in N2a cells after 24 h 12.5 $\mu\text{g/ml}$ 3-5
5
6
7 nm AgNPs treatment. The control groups (A-D) and AgNPs exposure groups (F-I)
8
9
10 were taken under 100X magnification respectively at 172 ms, 120 ms and 500 ms
11
12
13 exposure time for bright field (BF), hoechst, and primary rabbit anti-mouse $A\beta_{1-40}$. (E)
14
15
16 and (J) were a single cell image respectively according to (D) and (I) fields taken under
17
18
19 400X magnification. The white arrows pointed out the view of 400X images where are
20
21
22
23 selected from 100X ones.
24
25
26
27
28

Fig. 5 Amyloid- β_{1-42} plaques inside mouse neuron N2a cells in exposure to AgNPs.

29 Immunofluorescent detection of primary rabbit anti-mouse $A\beta_{1-42}$ was stained with
30
31
32 secondary goat FITC-conjugated anti-rabbit IgG in N2a cells after 24 h 12.5 $\mu\text{g/ml}$ 3-5
33
34
35 nm AgNPs treatment. The control groups (A-D) and AgNPs exposure groups (F-I)
36
37
38 were taken under 100X magnification respectively at 172 ms, 120 ms and 500 ms
39
40
41 exposure time for bright field (BF), hoechst, and primary rabbit anti-mouse $A\beta_{1-42}$. (E)
42
43
44 and (J) were a single cell image respectively according to (D) and (I) fields taken under
45
46
47
48 400X magnification. The white arrows pointed out the view of 400X images where are
49
50
51
52 selected from 100X ones.
53
54
55
56
57
58
59
60

Fig. 6 Quantitative changes of (A) *CXCL13*, (B) *MARCO*, (C) *GSS*, (D) *APP*, (E)

61 *LDLR* and (F) *NEP* gene expression in the neural cells with the treatment of 3-5 nm
62
63
64
65

1 AgNPs or LPS. Neural cells were treated with different concentration of 3-5 nm
2 AgNPs (0.5, 1, 5, 10 and 12.5 $\mu\text{g}/\text{ml}$) and LPS (ALT 2 $\mu\text{g}/\text{ml}$, BV-2 0.2 $\mu\text{g}/\text{ml}$ and N2a
3
4 2 $\mu\text{g}/\text{ml}$) for 24 h. The data were presented as mean \pm SD (n=3). *indicates significant
5
6
7 difference at $p < 0.05$ compared with control. ALT: astrocyte, BV-2: microglia, N2a:
8
9
10 neuron cells.

11
12
13
14
15
16 **Fig. 7** Protein levels of APP, LDLR and NEP in N2a cells after AgNPs exposure. The
17
18 total protein were 40, 40 and 100 μg individually loaded for immunoblotting to
19
20 determine (A) APP, (B) LDLR and (C) NEP in N2a cells exposed to 1, 5, 10, 12.5 and
21
22
23 15 $\mu\text{g}/\text{ml}$ AgNPs for 24 h, and quantified by ImageJ. *indicates significant difference at
24
25
26
27
28
29
30 $p < 0.05$ compared with control.

31
32
33
34
35
36 **Fig. 8** A schematic diagram of AgNPs exposure in brain neural cells to alter gene
37
38 expression potentially resulting in the progression of A β plaque deposition and
39
40 pathological feature of Alzheimer's disease. AgNPs can enter across neuronal cell
41
42 membrane and induce the gene expression of *CXCL13*, *MARCO* and *GSS* in response
43
44
45 to inflammatory reaction and oxidative stress. Sequentially, *APP* gene is activated for
46
47
48 A β amyloid production, ApoE transport is influenced to accelerate A β aggregation, and
49
50
51
52
53
54
55
56
57
58
59
60
61
62
63
64
65
66
67
68
69
70
71
72
73
74
75
76
77
78
79
80
81
82
83
84
85
86
87
88
89
90
91
92
93
94
95
96
97
98
99
100
101
102
103
104
105
106
107
108
109
110
111
112
113
114
115
116
117
118
119
120
121
122
123
124
125
126
127
128
129
130
131
132
133
134
135
136
137
138
139
140
141
142
143
144
145
146
147
148
149
150
151
152
153
154
155
156
157
158
159
160
161
162
163
164
165
166
167
168
169
170
171
172
173
174
175
176
177
178
179
180
181
182
183
184
185
186
187
188
189
190
191
192
193
194
195
196
197
198
199
200
201
202
203
204
205
206
207
208
209
210
211
212
213
214
215
216
217
218
219
220
221
222
223
224
225
226
227
228
229
230
231
232
233
234
235
236
237
238
239
240
241
242
243
244
245
246
247
248
249
250
251
252
253
254
255
256
257
258
259
260
261
262
263
264
265
266
267
268
269
270
271
272
273
274
275
276
277
278
279
280
281
282
283
284
285
286
287
288
289
290
291
292
293
294
295
296
297
298
299
300
301
302
303
304
305
306
307
308
309
310
311
312
313
314
315
316
317
318
319
320
321
322
323
324
325
326
327
328
329
330
331
332
333
334
335
336
337
338
339
340
341
342
343
344
345
346
347
348
349
350
351
352
353
354
355
356
357
358
359
360
361
362
363
364
365
366
367
368
369
370
371
372
373
374
375
376
377
378
379
380
381
382
383
384
385
386
387
388
389
390
391
392
393
394
395
396
397
398
399
400
401
402
403
404
405
406
407
408
409
410
411
412
413
414
415
416
417
418
419
420
421
422
423
424
425
426
427
428
429
430
431
432
433
434
435
436
437
438
439
440
441
442
443
444
445
446
447
448
449
450
451
452
453
454
455
456
457
458
459
460
461
462
463
464
465
466
467
468
469
470
471
472
473
474
475
476
477
478
479
480
481
482
483
484
485
486
487
488
489
490
491
492
493
494
495
496
497
498
499
500
501
502
503
504
505
506
507
508
509
510
511
512
513
514
515
516
517
518
519
520
521
522
523
524
525
526
527
528
529
530
531
532
533
534
535
536
537
538
539
540
541
542
543
544
545
546
547
548
549
550
551
552
553
554
555
556
557
558
559
560
561
562
563
564
565
566
567
568
569
570
571
572
573
574
575
576
577
578
579
580
581
582
583
584
585
586
587
588
589
590
591
592
593
594
595
596
597
598
599
600
601
602
603
604
605
606
607
608
609
610
611
612
613
614
615
616
617
618
619
620
621
622
623
624
625
626
627
628
629
630
631
632
633
634
635
636
637
638
639
640
641
642
643
644
645
646
647
648
649
650
651
652
653
654
655
656
657
658
659
660
661
662
663
664
665
666
667
668
669
670
671
672
673
674
675
676
677
678
679
680
681
682
683
684
685
686
687
688
689
690
691
692
693
694
695
696
697
698
699
700
701
702
703
704
705
706
707
708
709
710
711
712
713
714
715
716
717
718
719
720
721
722
723
724
725
726
727
728
729
730
731
732
733
734
735
736
737
738
739
740
741
742
743
744
745
746
747
748
749
750
751
752
753
754
755
756
757
758
759
760
761
762
763
764
765
766
767
768
769
770
771
772
773
774
775
776
777
778
779
780
781
782
783
784
785
786
787
788
789
790
791
792
793
794
795
796
797
798
799
800
801
802
803
804
805
806
807
808
809
810
811
812
813
814
815
816
817
818
819
820
821
822
823
824
825
826
827
828
829
830
831
832
833
834
835
836
837
838
839
840
841
842
843
844
845
846
847
848
849
850
851
852
853
854
855
856
857
858
859
860
861
862
863
864
865
866
867
868
869
870
871
872
873
874
875
876
877
878
879
880
881
882
883
884
885
886
887
888
889
890
891
892
893
894
895
896
897
898
899
900
901
902
903
904
905
906
907
908
909
910
911
912
913
914
915
916
917
918
919
920
921
922
923
924
925
926
927
928
929
930
931
932
933
934
935
936
937
938
939
940
941
942
943
944
945
946
947
948
949
950
951
952
953
954
955
956
957
958
959
960
961
962
963
964
965
966
967
968
969
970
971
972
973
974
975
976
977
978
979
980
981
982
983
984
985
986
987
988
989
990
991
992
993
994
995
996
997
998
999
1000

response and A β amyloid deposition might evolve neurodegenerative Alzheimer's
disease. The number and arrow marked in red are fold-change levels and up-/down-
regulation of gene expression.

1
2
3
4
5
6
7
8
9
10
11
12
13
14
15
16
17
18
19
20
21
22
23
24
25
26
27
28
29
30
31
32
33
34
35
36
37
38
39
40
41
42
43
44
45
46
47
48
49
50
51
52
53
54
55
56
57
58
59
60
61
62
63
64
65

References

- 1 BASAK, J. M., VERGHESE, P. B., YOON, H., KIM, J. & HOLTZMAN, D. M. 2012.
2 Low-density lipoprotein receptor represents an apolipoprotein E-independent
3 pathway of Abeta uptake and degradation by astrocytes. *J Biol Chem*, 287,
4 13959-71.
5
6 CAMERON, B. & LANDRETH, G. E. 2010. Inflammation, microglia, and Alzheimer's
7 disease. *Neurobiol Dis*, 37, 503-9.
8
9 CAO, D., FUKUCHI, K., WAN, H., KIM, H. & LI, L. 2006. Lack of LDL receptor aggravates
10 learning deficits and amyloid deposits in Alzheimer transgenic mice. *Neurobiol*
11 *Aging*, 27, 1632-43.
12
13 CHA, K., HONG, H. W., CHOI, Y. G., LEE, M. J., PARK, J. H., CHAE, H. K., RYU, G. &
14 MYUNG, H. 2008. Comparison of acute responses of mice livers to short-term
15 exposure to nano-sized or micro-sized silver particles. *Biotechnol Lett*, 30,
16 1893-9.
17
18 CHRISTEN, V., CAPELLE, M. & FENT, K. 2013. Silver nanoparticles induce endoplasmatic
19 reticulum stress response in zebrafish. *Toxicol Appl Pharmacol*, 272, 519-28.
20
21 DONG, S., DUAN, Y., HU, Y. & ZHAO, Z. 2012. Advances in the pathogenesis of
22 Alzheimer's disease: a re-evaluation of amyloid cascade hypothesis. *Transl*
23 *Neurodegener*, 1, 18.
24
25 DZIENDZIKOWSKA, K., GROMADZKA-OSTROWSKA, J., LANKOFF, A., OCZKOWSKI, M.,
26 KRAWCZYNSKA, A., CHWASTOWSKA, J., SADOWSKA-BRATEK, M., CHAJDUK, E.,
27 WOJEWODZKA, M., DUSINSKA, M. & KRUSZEWSKI, M. 2012. Time-dependent
28 biodistribution and excretion of silver nanoparticles in male Wistar rats. *J Appl*
29 *Toxicol*, 32, 920-8.
30
31 EL-AMOURI, S. S., ZHU, H., YU, J., GAGE, F. H., VERMA, I. M. & KINDY, M. S. 2007.
32 Neprilysin protects neurons against Abeta peptide toxicity. *Brain Res*, 1152,
33 191-200.
34
35 EOM, H. J. & CHOI, J. 2010. p38 MAPK activation, DNA damage, cell cycle arrest and
36 apoptosis as mechanisms of toxicity of silver nanoparticles in Jurkat T cells.
37 *Environ Sci Technol*, 44, 8337-42.
38
39 FOLDBJERG, R., DANG, D. A. & AUTRUP, H. 2011. Cytotoxicity and genotoxicity of silver
40 nanoparticles in the human lung cancer cell line, A549. *Arch Toxicol*, 85, 743-50.
41
42 GAISER, B. K., HIRN, S., KERMANIZADEH, A., KANASE, N., FYTIANOS, K., WENK, A.,
43 HABERL, N., BRUNELLI, A., KREYLING, W. G. & STONE, V. 2013. Effects of silver
44 nanoparticles on the liver and hepatocytes in vitro. *Toxicol Sci*, 131, 537-47.
45
46 HAASE, A., ROTT, S., MANTION, A., GRAF, P., PLENDL, J., THUNEMANN, A. F., MEIER, W.
47 P., TAUBERT, A., LUCH, A. & REISER, G. 2012. Effects of silver nanoparticles on
48 primary mixed neural cell cultures: uptake, oxidative stress and acute calcium
49 responses. *Toxicol Sci*, 126, 457-68.
50
51 HAN, S. H., KIM, Y. H. & MOOK-JUNG, I. 2011. RAGE: the beneficial and deleterious
52 effects by diverse mechanisms of actions. *Mol Cells*, 31, 91-7.
53
54 HOHNHOLT, M. C., GEPPERT, M., LUTHER, E. M., PETTERS, C., BULCKE, F. & DRINGEN, R.
55 2013. Handling of iron oxide and silver nanoparticles by astrocytes. *Neurochem*
56
57
58
59
60
61
62
63
64
65

Res, 38, 227-39.

- 1
2
3
4
5
6
7
8
9
10
11
12
13
14
15
16
17
18
19
20
21
22
23
24
25
26
27
28
29
30
31
32
33
34
35
36
37
38
39
40
41
42
43
44
45
46
47
48
49
50
51
52
53
54
55
56
57
58
59
60
61
62
63
64
65
- KANEKIYO, T., LIU, C. C., SHINOHARA, M., LI, J. & BU, G. 2012. LRP1 in brain vascular smooth muscle cells mediates local clearance of Alzheimer's amyloid-beta. *J Neurosci*, 32, 16458-65.
- KANG, S. J., LEE, Y. J., LEE, E. K. & KWAK, M. K. 2012. Silver nanoparticles-mediated G2/M cycle arrest of renal epithelial cells is associated with NRF2-GSH signaling. *Toxicol Lett*, 211, 334-41.
- KOIKE, S., OGASAWARA, Y., SHIBUYA, N., KIMURA, H. & ISHII, K. 2013. Polysulfide exerts a protective effect against cytotoxicity caused by t-buthylhydroperoxide through Nrf2 signaling in neuroblastoma cells. *FEBS Lett*, 587, 3548-55.
- KOMINE, H., KUHN, L., MATSUSHITA, N., MULE, J. J. & PILON-THOMAS, S. 2013. Examination of MARCO activity on dendritic cell phenotype and function using a gene knockout mouse. *PLoS One*, 8, e67795.
- KULTHONG, K., SRISUNG, S., BOONPAVANITCHAKUL, K., KANGWANSUPAMONKON, W. & MANIRATANACHOTE, R. 2010. Determination of silver nanoparticle release from antibacterial fabrics into artificial sweat. *Part Fibre Toxicol*, 7, 8.
- LANDAU, S. M., LU, M., JOSHI, A. D., PONTECORVO, M., MINTUN, M. A., TROJANOWSKI, J. Q., SHAW, L. M., JAGUST, W. J. & ALZHEIMER'S DISEASE NEUROIMAGING, I. 2013. Comparing positron emission tomography imaging and cerebrospinal fluid measurements of beta-amyloid. *Ann Neurol*, 74, 826-36.
- LEE, D. Y., FORTIN, C. & CAMPBELL, P. G. 2005. Contrasting effects of chloride on the toxicity of silver to two green algae, *Pseudokirchneriella subcapitata* and *Chlamydomonas reinhardtii*. *Aquat Toxicol*, 75, 127-35.
- LOO, S. L., FANE, A. G., LIM, T. T., KRANTZ, W. B., LIANG, Y. N., LIU, X. & HU, X. 2013. Superabsorbent Cryogels Decorated with Silver Nanoparticles as a Novel Water Technology for Point-of-Use Disinfection. *Environ Sci Technol*, 47, 9363-71.
- MERAZ-RIOS, M. A., TORAL-RIOS, D., FRANCO-BOCANEGRA, D., VILLEDA-HERNANDEZ, J. & CAMPOS-PENA, V. 2013. Inflammatory process in Alzheimer's Disease. *Front Integr Neurosci*, 7, 59.
- MORRIS, J. C., ROE, C. M., XIONG, C., FAGAN, A. M., GOATE, A. M., HOLTZMAN, D. M. & MINTUN, M. A. 2010. APOE predicts amyloid-beta but not tau Alzheimer pathology in cognitively normal aging. *Ann Neurol*, 67, 122-31.
- NAKAJIMA, T., AMANUMA, R., UEKI-MARUYAMA, K., ODA, T., HONDA, T., ITO, H. & YAMAZAKI, K. 2008. CXCL13 expression and follicular dendritic cells in relation to B-cell infiltration in periodontal disease tissues. *J Periodontal Res*, 43, 635-41.
- PARK, M. H., LEE, J. K., CHOI, S., AHN, J., JIN, H. K., PARK, J. S. & BAE, J. S. 2013. Recombinant soluble neprilysin reduces amyloid-beta accumulation and improves memory impairment in Alzheimer's disease mice. *Brain Res*, 1529, 113-24.
- PRASAD, R. Y., MCGEE, J. K., KILLIUS, M. G., SUAREZ, D. A., BLACKMAN, C. F., DEMARINI, D. M. & SIMMONS, S. O. 2013. Investigating oxidative stress and inflammatory responses elicited by silver nanoparticles using high-throughput reporter genes in HepG2 cells: effect of size, surface coating, and intracellular uptake. *Toxicol In Vitro*, 27, 2013-21.

- 1
2
3
4
5
6
7
8
9
10
11
12
13
14
15
16
17
18
19
20
21
22
23
24
25
26
27
28
29
30
31
32
33
34
35
36
37
38
39
40
41
42
43
44
45
46
47
48
49
50
51
52
53
54
55
56
57
58
59
60
61
62
63
64
65
- QUADROS, M. E. & MARR, L. C. 2010. Environmental and human health risks of aerosolized silver nanoparticles. *J Air Waste Manag Assoc*, 60, 770-81.
- RAHMAN, M. F., WANG, J., PATTERSON, T. A., SAINI, U. T., ROBINSON, B. L., NEWPORT, G. D., MURDOCK, R. C., SCHLAGER, J. J., HUSSAIN, S. M. & ALI, S. F. 2009. Expression of genes related to oxidative stress in the mouse brain after exposure to silver-25 nanoparticles. *Toxicol Lett*, 187, 15-21.
- RIBEIRO, F., GALLEGU-URREA, J. A., JURKSCHAT, K., CROSSLEY, A., HASSELLOV, M., TAYLOR, C., SOARES, A. M. & LOUREIRO, S. 2013. Silver nanoparticles and silver nitrate induce high toxicity to *Pseudokirchneriella subcapitata*, *Daphnia magna* and *Danio rerio*. *Sci Total Environ*, 466-467C, 232-241.
- SELENICA, M. L., ALVAREZ, J. A., NASH, K. R., LEE, D. C., CAO, C., LIN, X., REID, P., MOUTON, P. R., MORGAN, D. & GORDON, M. N. 2013. Diverse activation of microglia by chemokine (C-C motif) ligand 2 overexpression in brain. *J Neuroinflammation*, 10, 86.
- SHARMA, H. S. & SHARMA, A. 2012. Neurotoxicity of engineered nanoparticles from metals. *CNS Neurol Disord Drug Targets*, 11, 65-80.
- SINGH, R. P. & RAMARAO, P. 2012. Cellular uptake, intracellular trafficking and cytotoxicity of silver nanoparticles. *Toxicol Lett*, 213, 249-59.
- SMITH, M. P. & CASS, W. A. 2007. Oxidative stress and dopamine depletion in an intrastriatal 6-hydroxydopamine model of Parkinson's disease. *Neuroscience*, 144, 1057-66.
- SOFRONIEW, M. V. & VINTERS, H. V. 2010. Astrocytes: biology and pathology. *Acta Neuropathol*, 119, 7-35.
- TANG, J., XIONG, L., WANG, S., WANG, J., LIU, L., LI, J., YUAN, F. & XI, T. 2009. Distribution, translocation and accumulation of silver nanoparticles in rats. *J Nanosci Nanotechnol*, 9, 4924-32.
- TANG, J., XIONG, L., ZHOU, G., WANG, S., WANG, J., LIU, L., LI, J., YUAN, F., LU, S., WAN, Z., CHOU, L. & XI, T. 2010. Silver nanoparticles crossing through and distribution in the blood-brain barrier in vitro. *J Nanosci Nanotechnol*, 10, 6313-7.
- TAPPIN, A. D., BARRIADA, J. L., BRAUNGARDT, C. B., EVANS, E. H., PATEY, M. D. & ACHTERBERG, E. P. 2010. Dissolved silver in European estuarine and coastal waters. *Water Res*, 44, 4204-16.
- VERANO-BRAGA, T., MIETHLING-GRAFF, R., WOJDYLA, K., ROGOWSKA-WRZESINSKA, A., BREWER, J. R., ERDMANN, H. & KJELDSEN, F. 2014. Insights into the cellular response triggered by silver nanoparticles using quantitative proteomics. *ACS Nano*, 8, 2161-75.
- WANG, S., WANG, R., CHEN, L., BENNETT, D. A., DICKSON, D. W. & WANG, D. S. 2010. Expression and functional profiling of neprilysin, insulin-degrading enzyme, and endothelin-converting enzyme in prospectively studied elderly and Alzheimer's brain. *J Neurochem*, 115, 47-57.
- WANG, Y., WANG, B., ZHU, M. T., LI, M., WANG, H. J., WANG, M., OUYANG, H., CHAI, Z. F., FENG, W. Y. & ZHAO, Y. L. 2011. Microglial activation, recruitment and phagocytosis as linked phenomena in ferric oxide nanoparticle exposure. *Toxicol Lett*, 205, 26-37.

- 1
2
3
4
5
6
7
8
9
10
11
12
13
14
15
16
17
18
19
20
21
22
23
24
25
26
27
28
29
30
31
32
33
34
35
36
37
38
39
40
41
42
43
44
45
46
47
48
49
50
51
52
53
54
55
56
57
58
59
60
61
62
63
64
65
- WEI, J., GABRUSIEWICZ, K. & HEIMBERGER, A. 2013. The controversial role of microglia in malignant gliomas. *Clin Dev Immunol*, 2013, 285246.
- WEISS, N., MILLER, F., CAZAUBON, S. & COURAUD, P. O. 2009. The blood-brain barrier in brain homeostasis and neurological diseases. *Biochim Biophys Acta*, 1788, 842-57.
- WIJNHOFEN, S. W. P., PEIJNENBURG, W. J. G. M., HERBERTS, C. A., HAGENS, W. I., OOMEN, A. G., HEUGENS, E. H. W., ROSZEK, B., BISSCHOPS, J., GOSENS, I., VAN DE MEENT, D., DEKKERS, S., DE JONG, W. H., VAN ZIJVERDEN, M., SIPS, A. J. A. M. & GEERTSMA, R. E. 2009. Nano-silver - a review of available data and knowledge gaps in human and environmental risk assessment. *Nanotoxicology*, 3, 109-U78.
- XU, F., PIETT, C., FARKAS, S., QAZZAZ, M. & SYED, N. I. 2013. Silver nanoparticles (AgNPs) cause degeneration of cytoskeleton and disrupt synaptic machinery of cultured cortical neurons. *Mol Brain*, 6, 29.
- XU, P. X., WANG, S. W., YU, X. L., SU, Y. J., WANG, T., ZHOU, W. W., ZHANG, H., WANG, Y. J. & LIU, R. T. 2014. Rutin improves spatial memory in Alzheimer's disease transgenic mice by reducing A β oligomer level and attenuating oxidative stress and neuroinflammation. *Behav Brain Res*, 264, 173-80.

Figure 1
[Click here to download high resolution image](#)

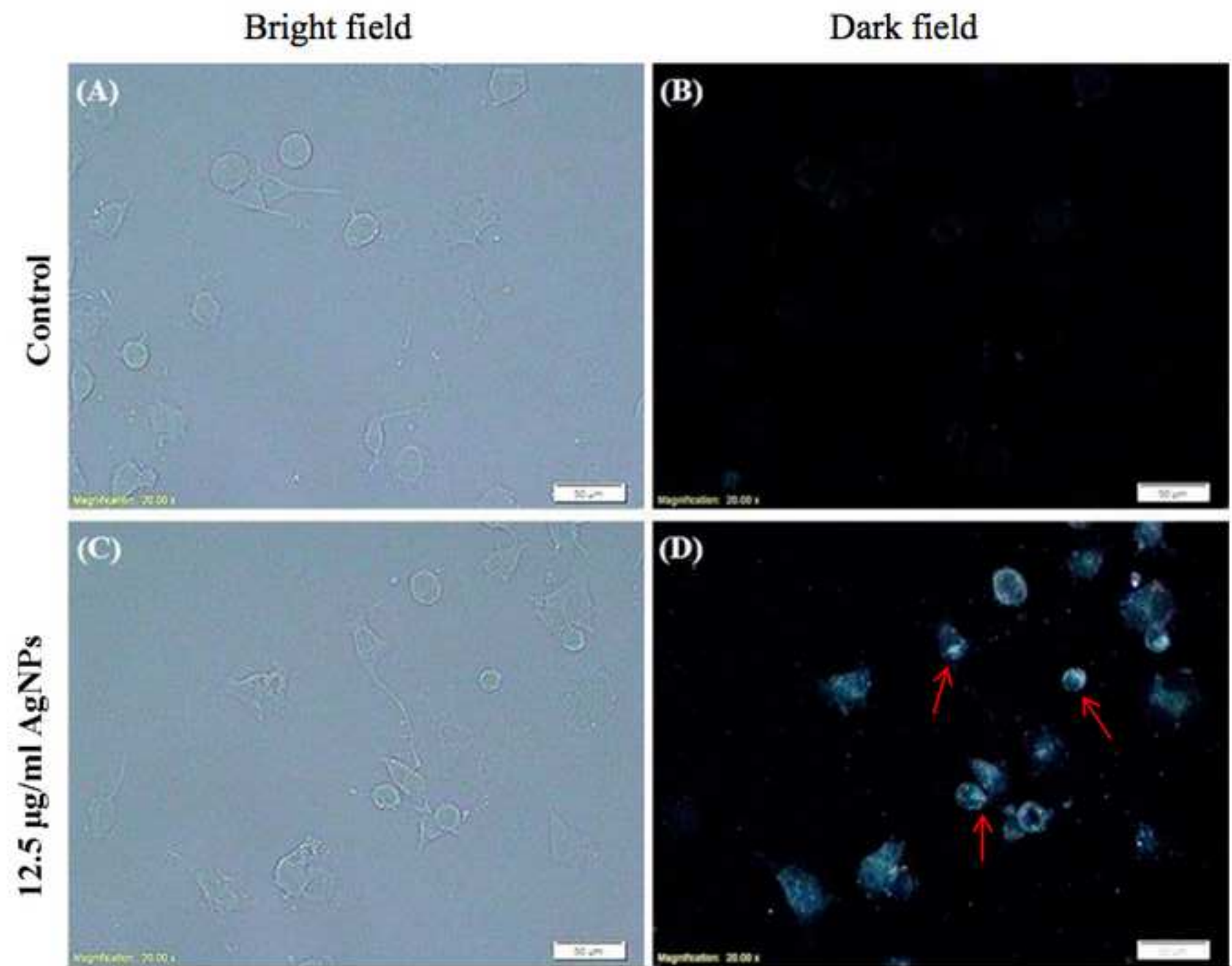


Fig. 2

[Click here to download high resolution image](#)

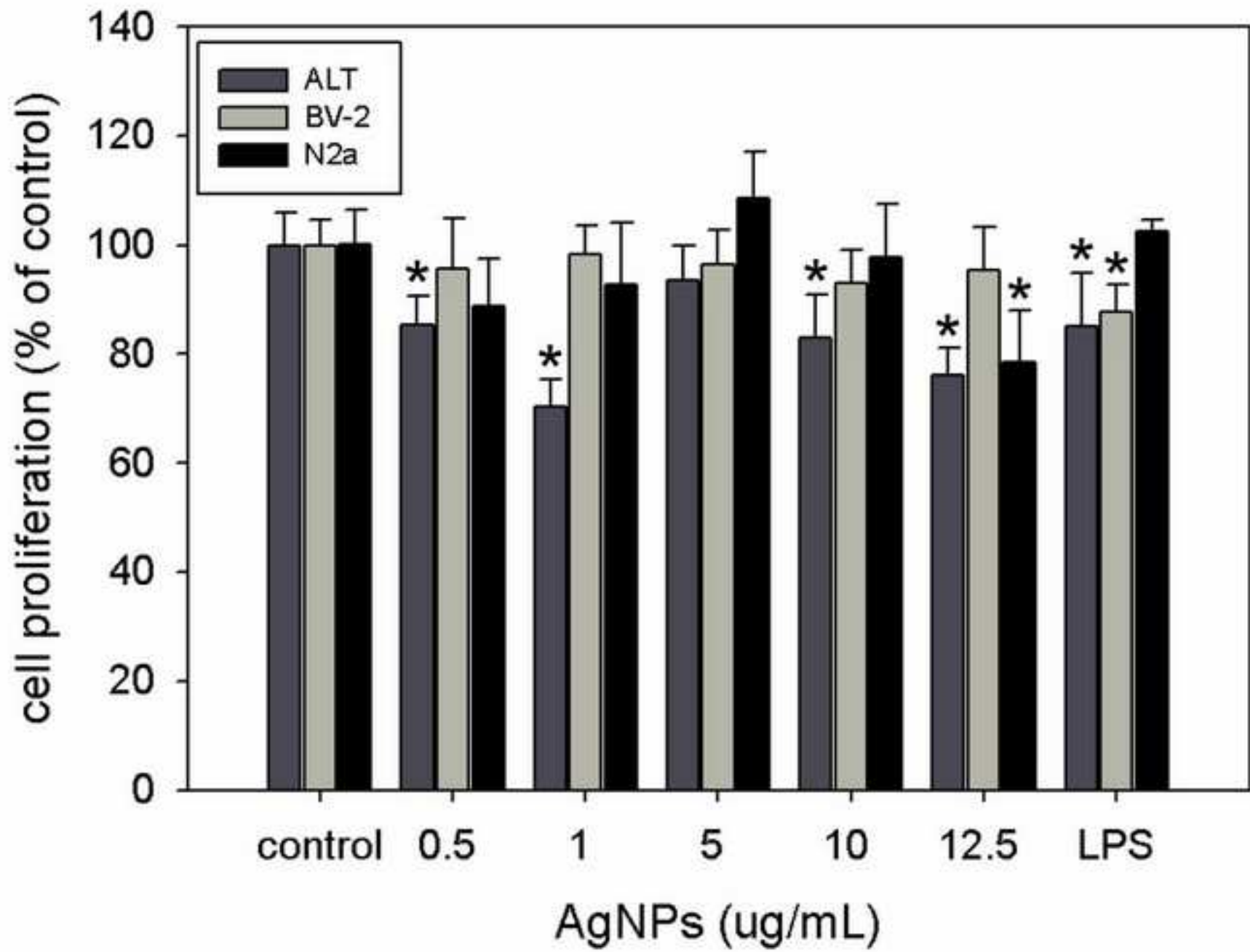
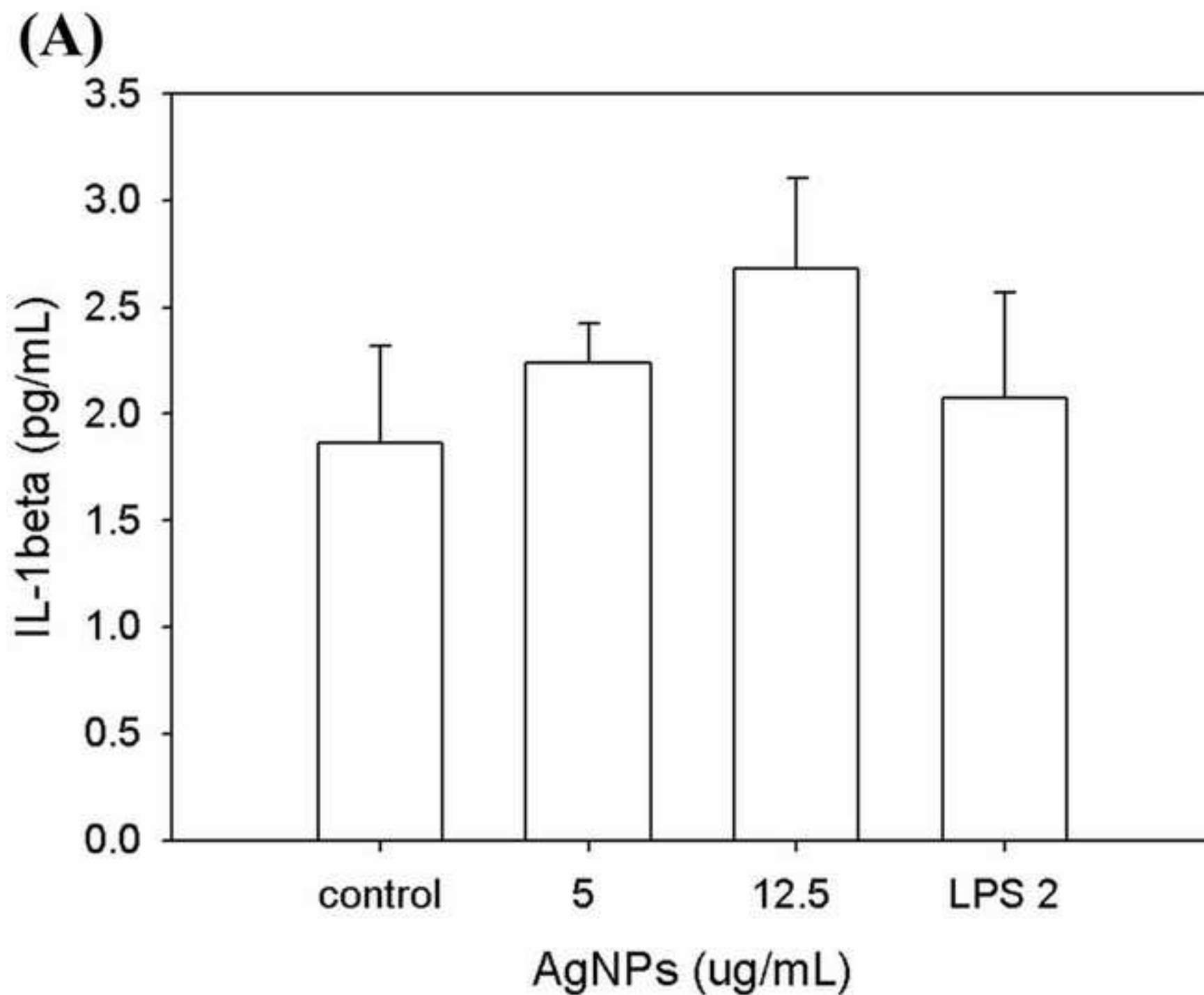


Fig. 3A

[Click here to download high resolution image](#)



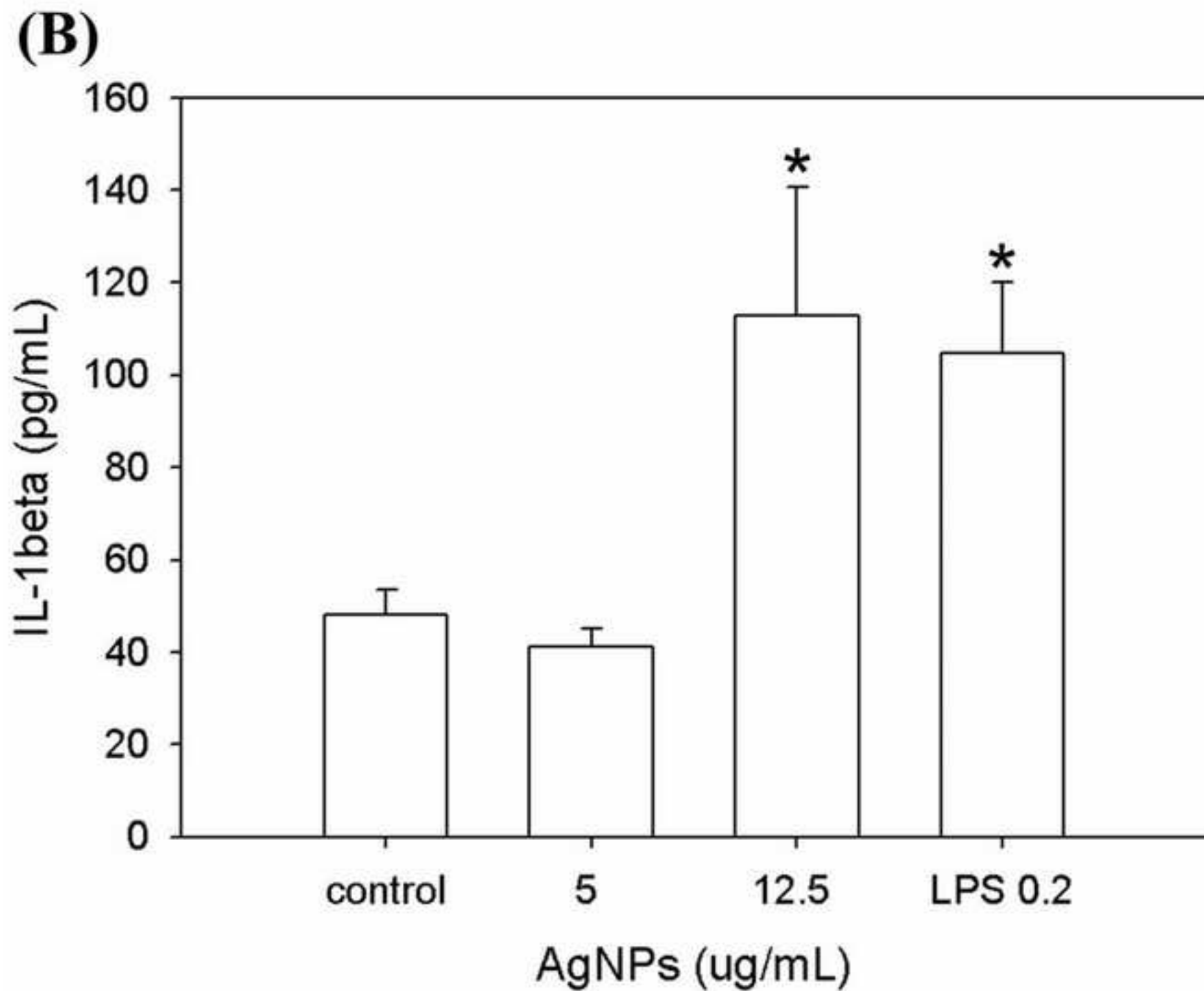


Fig. 3C
[Click here to download high resolution image](#)

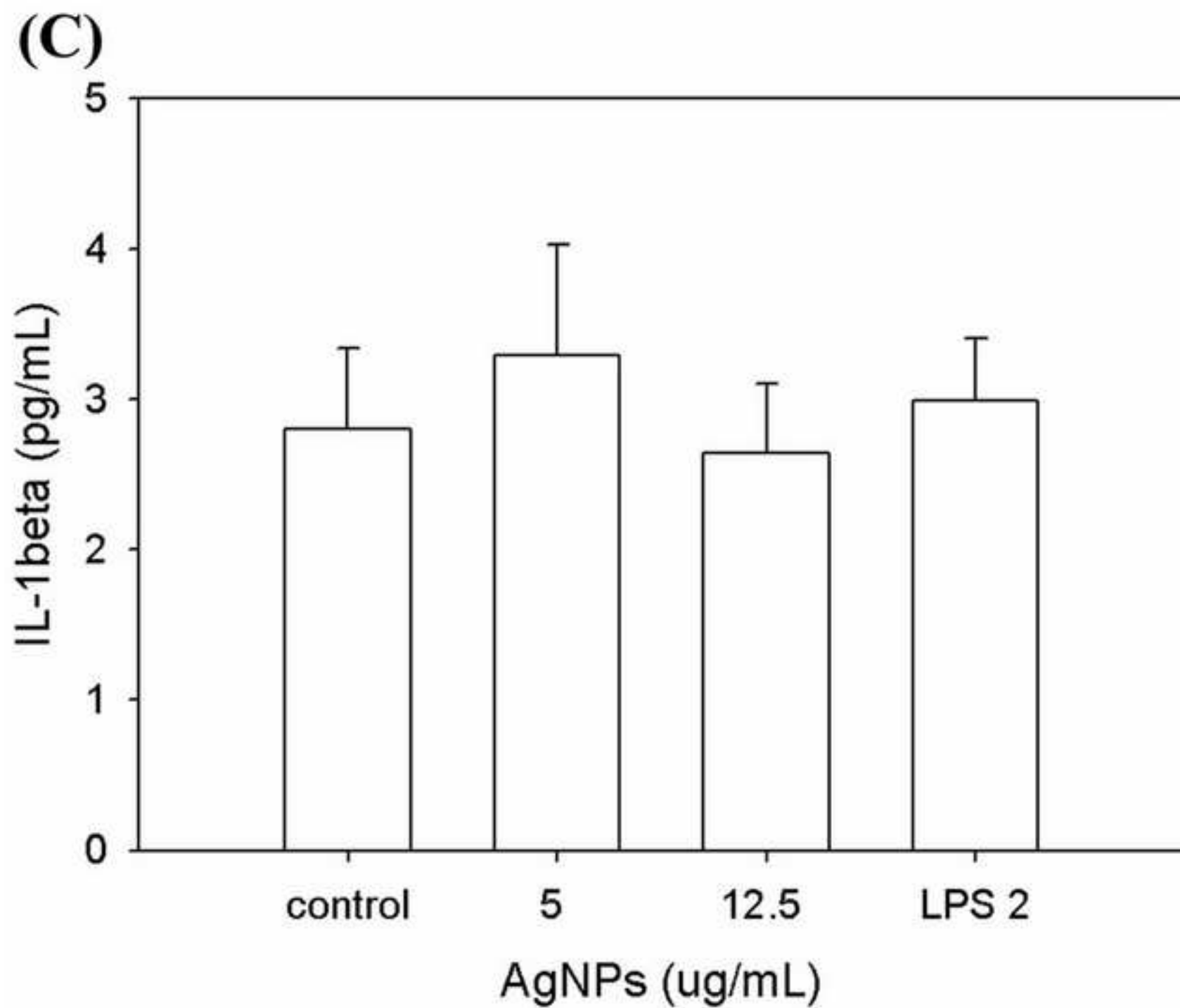


Figure 4
[Click here to download high resolution image](#)

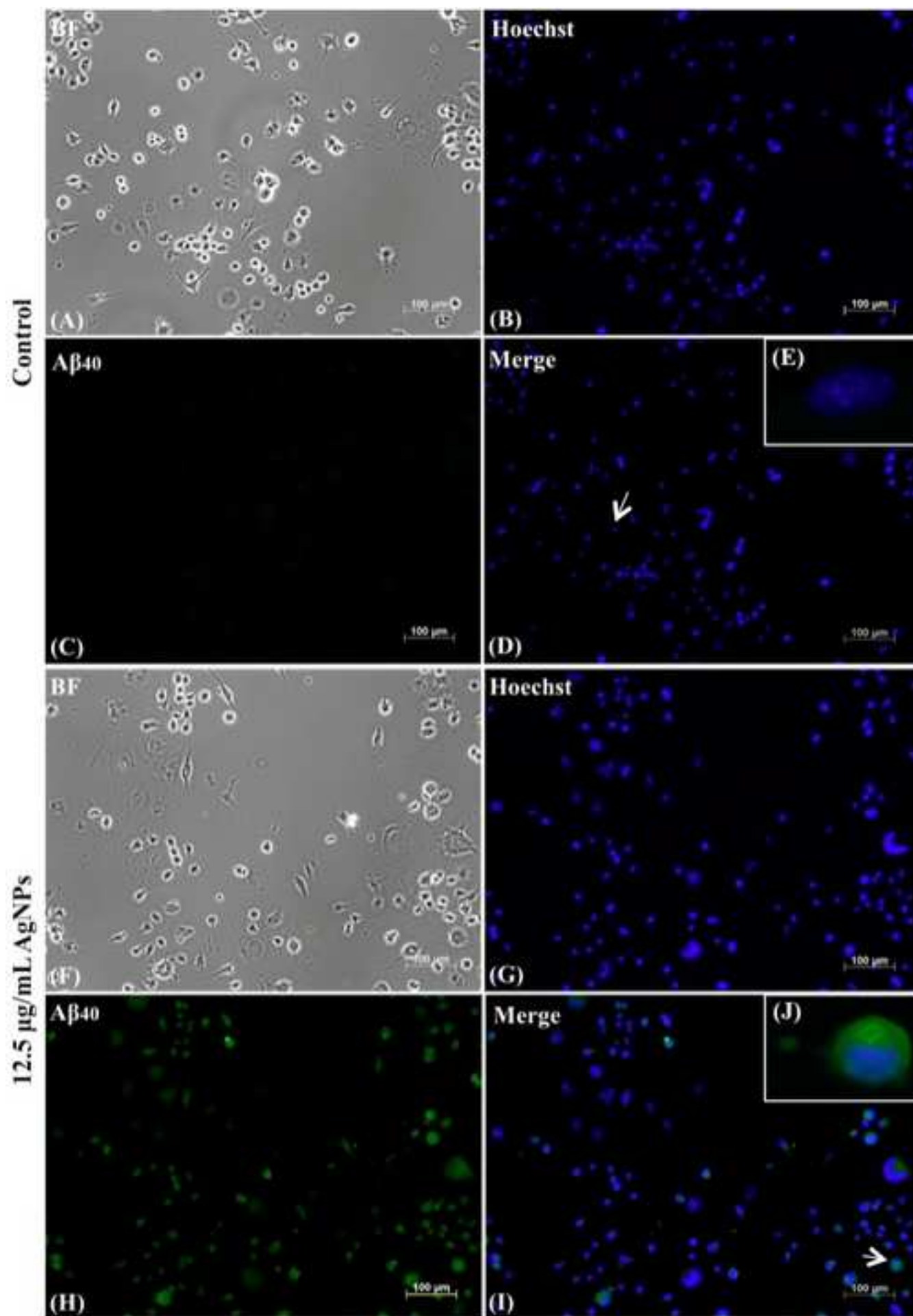


Figure 5

[Click here to download high resolution image](#)

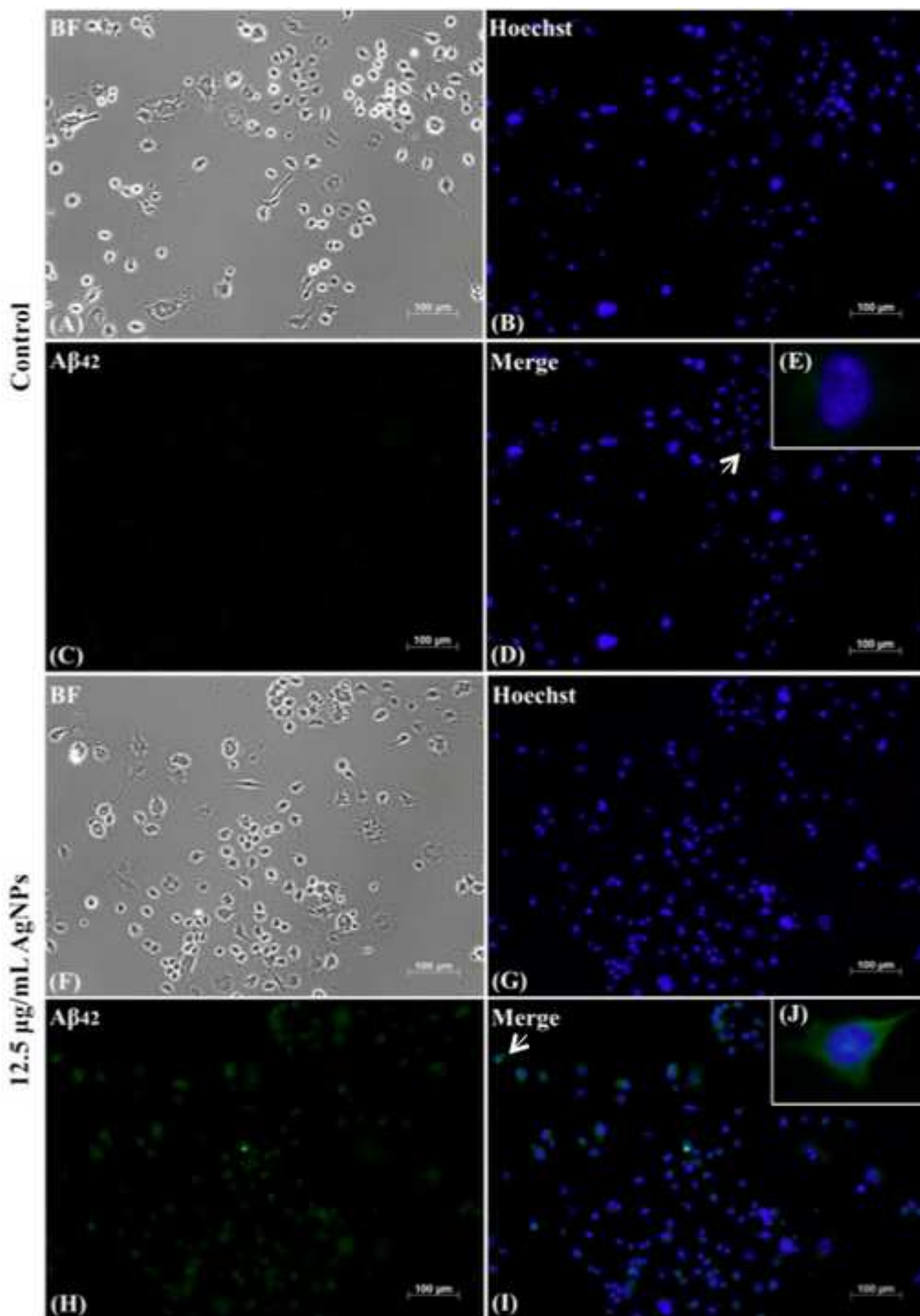


Fig. 6A

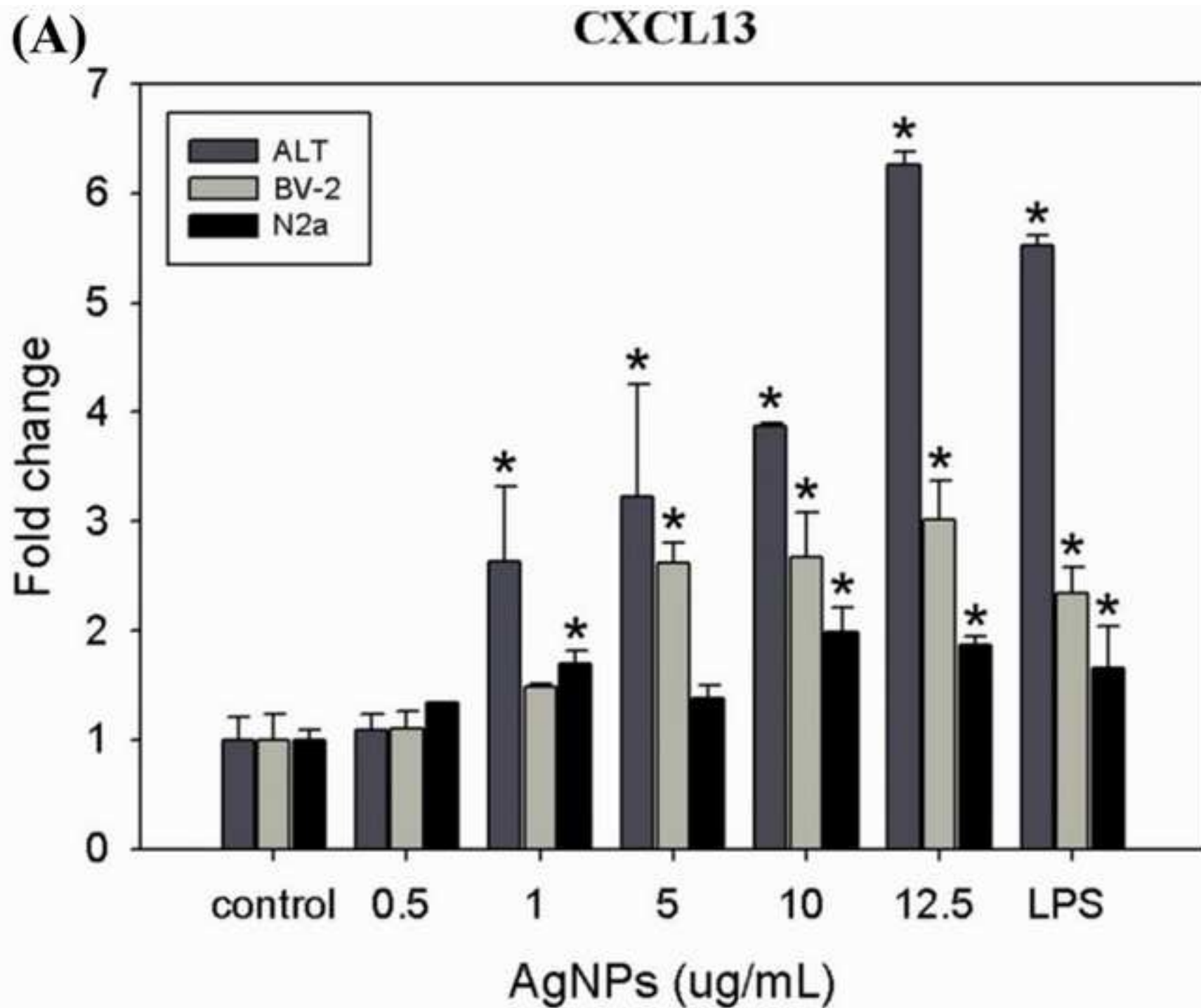
[Click here to download high resolution image](#)

Fig. 6B
[Click here to download high resolution image](#)

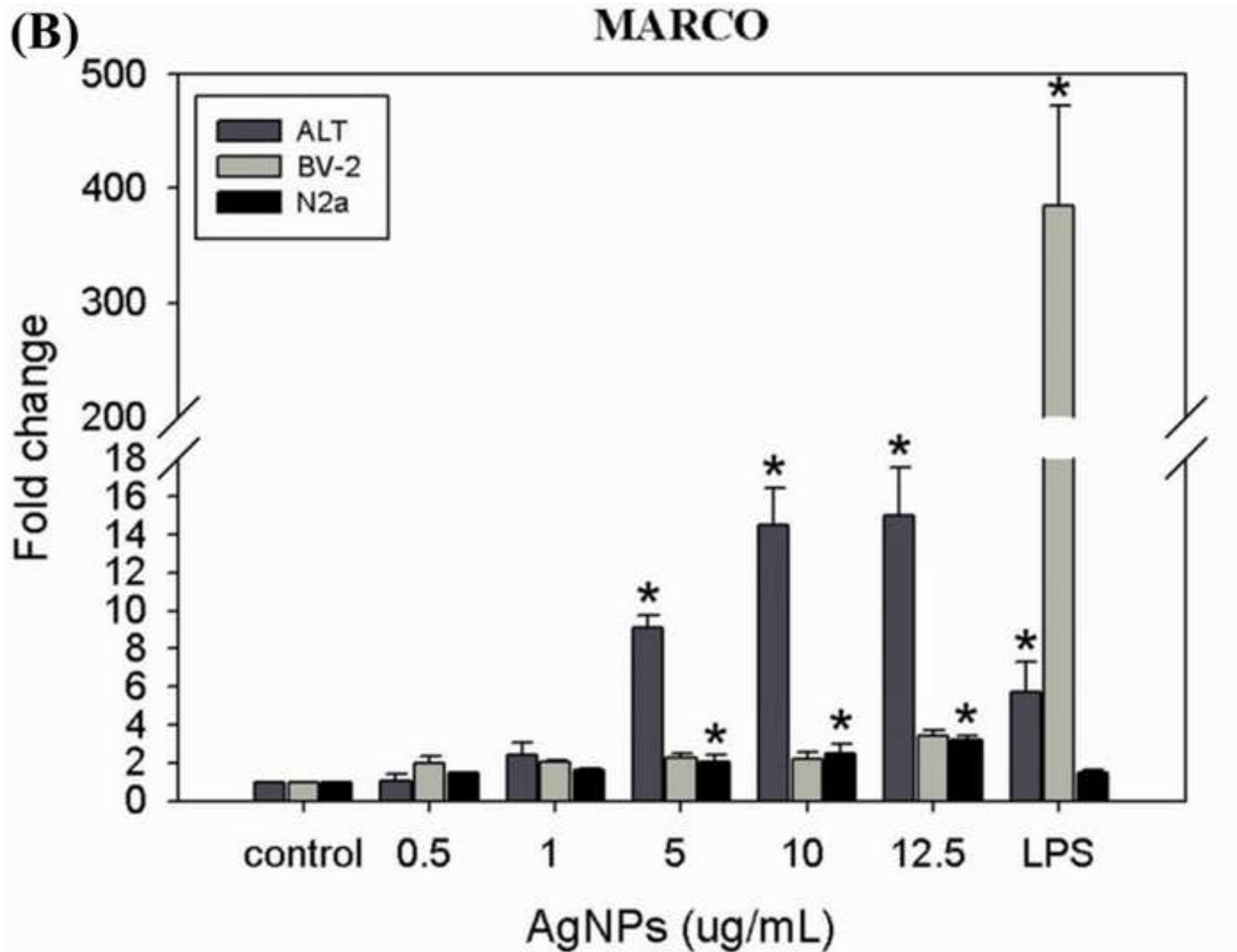


Fig. 6C
[Click here to download high resolution image](#)

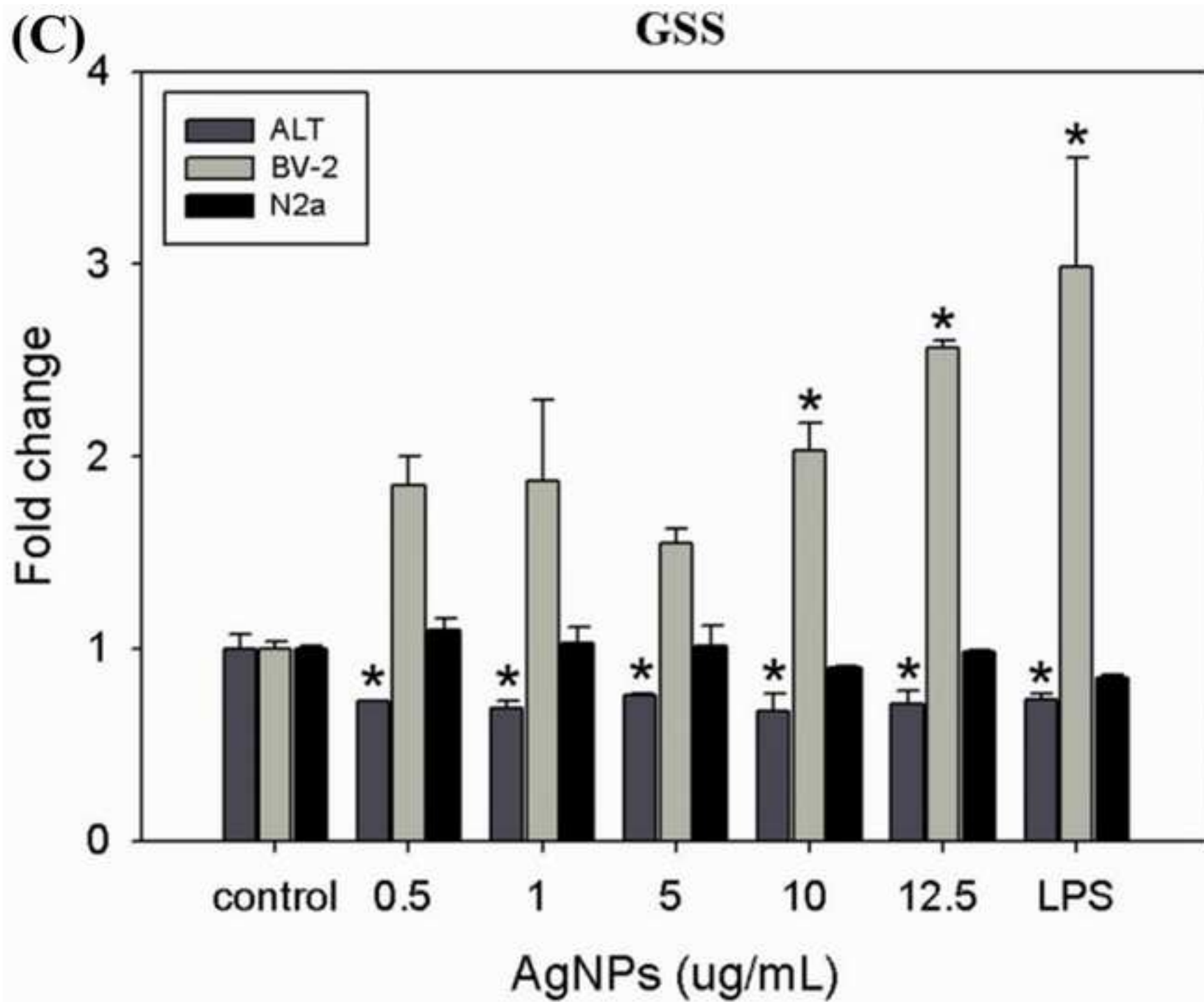
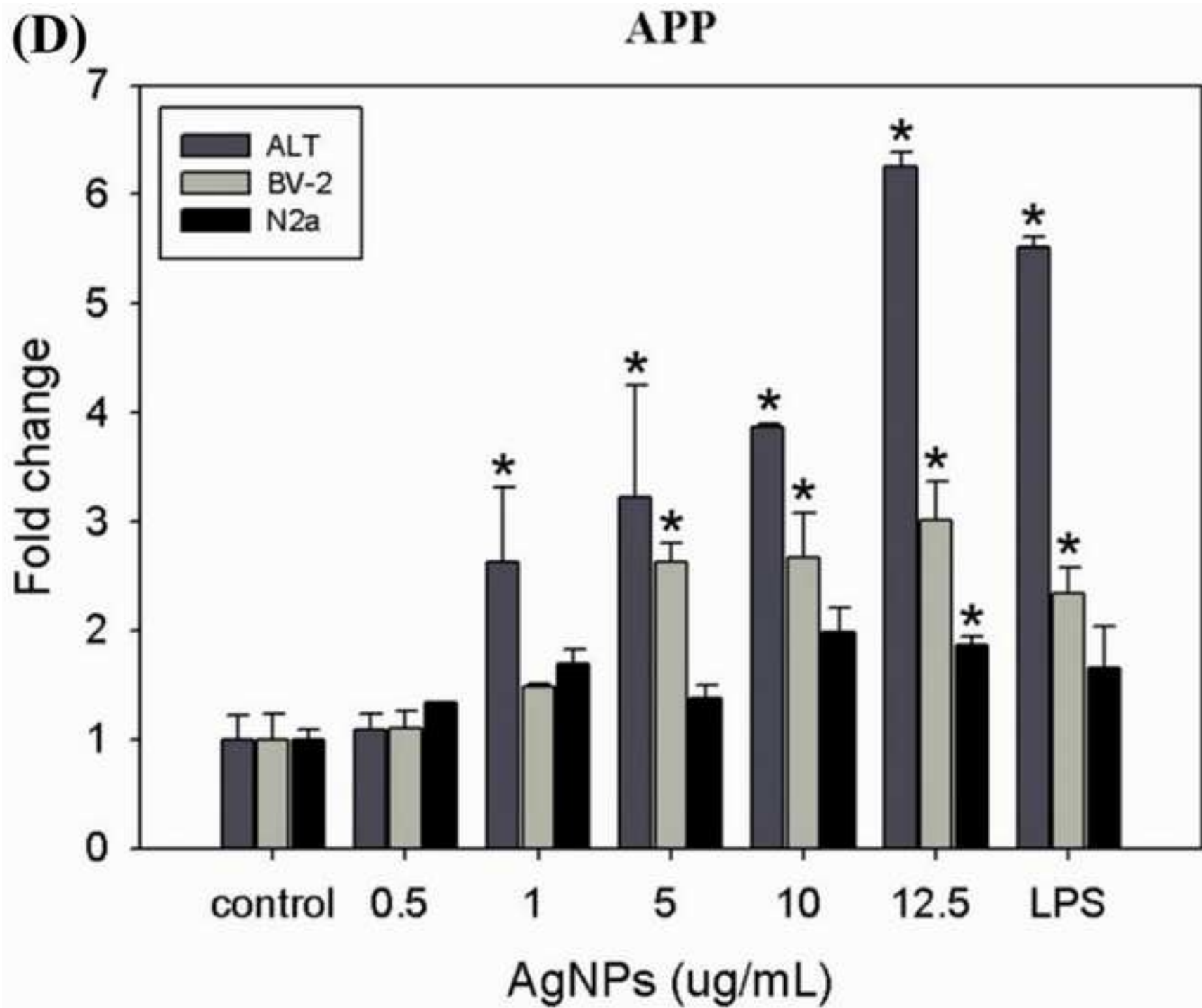


Fig. 6D

[Click here to download high resolution image](#)

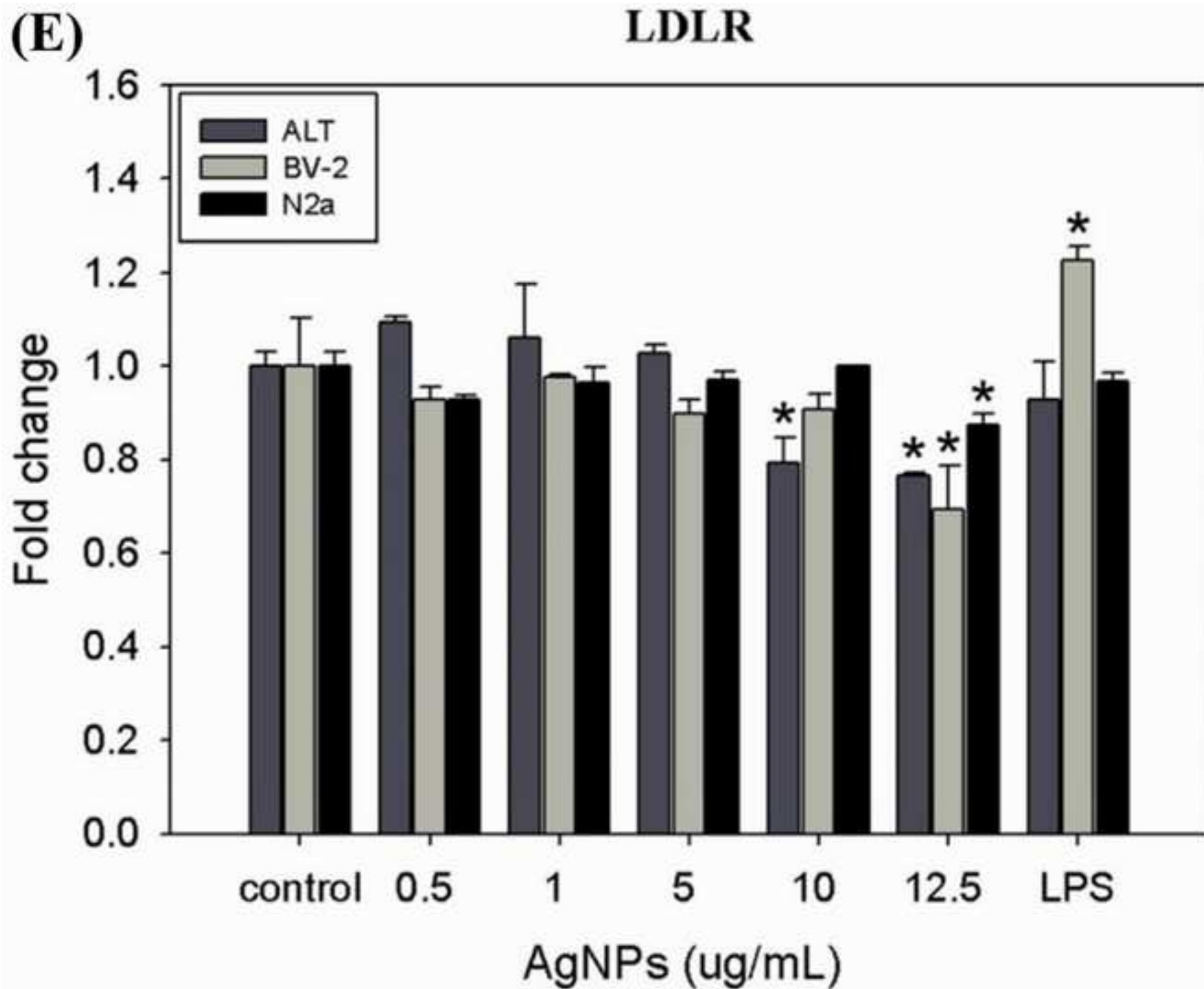


Fig. 6F
[Click here to download high resolution image](#)

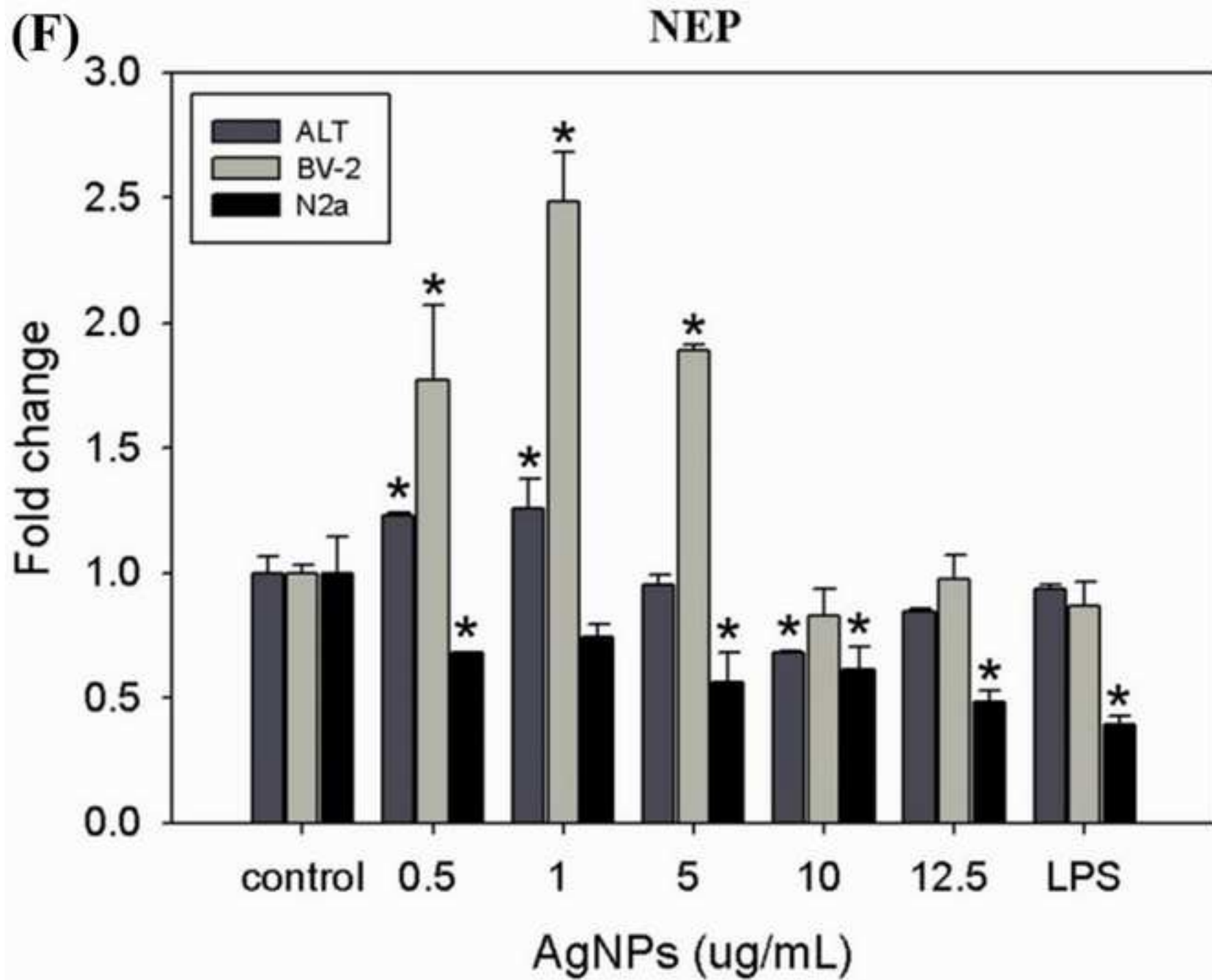


Figure 7
[Click here to download high resolution image](#)

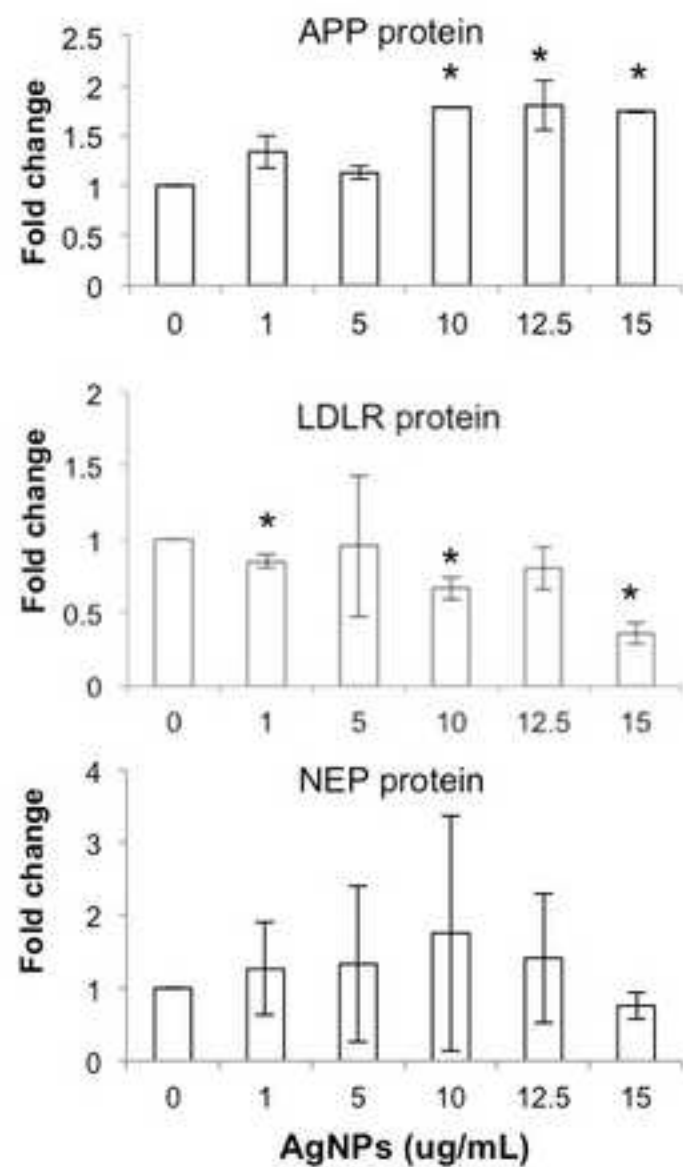
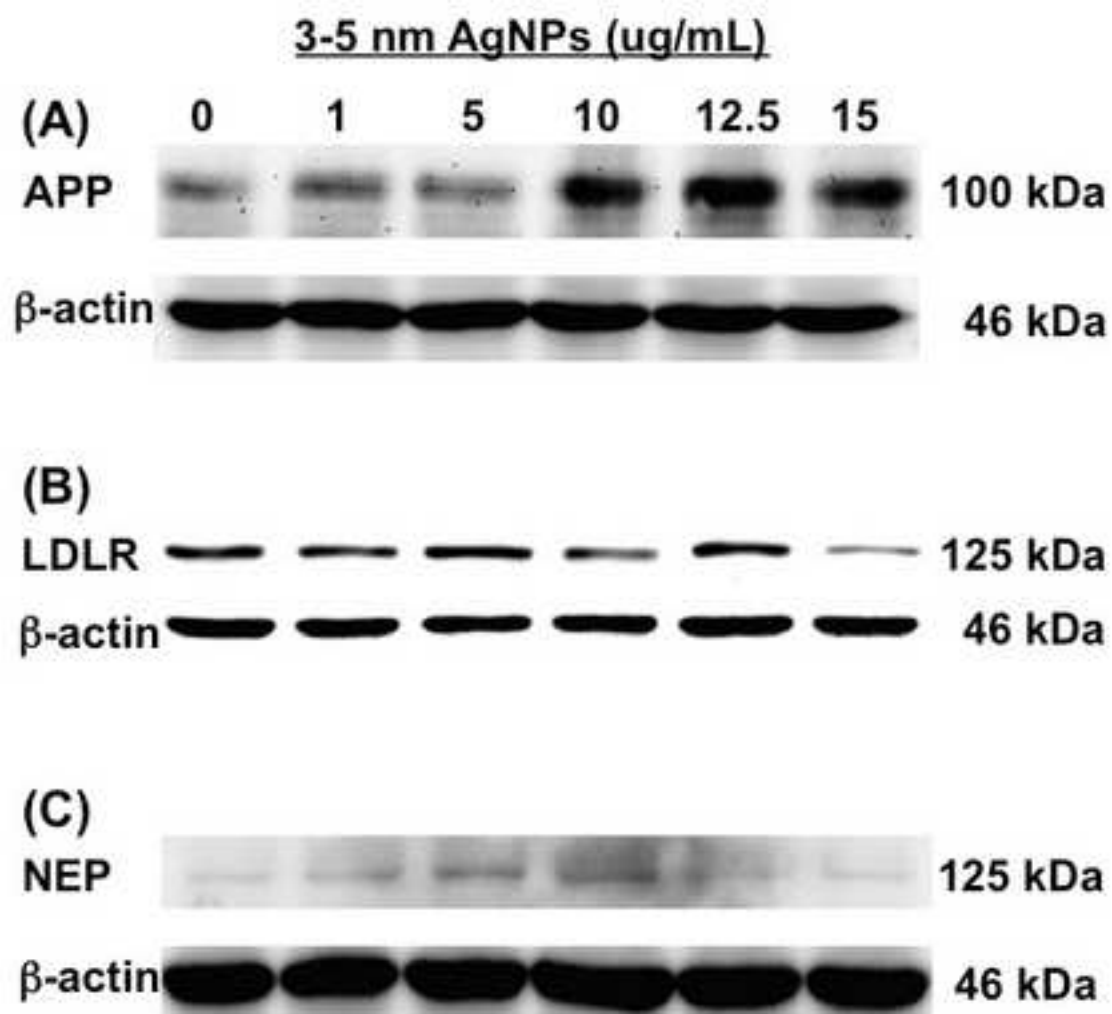


Figure 8
[Click here to download high resolution image](#)

